Peroxisomal import is circadian in glia and regulates sleep and lipid metabolism

Anurag Das[1,2]*, Irma Magaly Rivas-Serna[3], Ankur Kumar[1,4], Hia Kalita[5] Lakpa Sherpa[1,4], John P. Vaughen[6*], Hua Bai[1]*

1 Department of Genetics, Development, and Cell Biology, Iowa State University, Ames, IA 50011, USA
2 Interdepartmental Neuroscience PhD program, Iowa State University, Ames, IA 50011, USA
3 Department of Agriculture, Food, and Nutritional Science, University of Alberta; Edmonton, T6G 2R3, Canada.
4 Interdepartmental Genetics & Genomics PhD program, Iowa State University, Ames, IA 50011, USA
5 Interdepartmental MCDB PhD program, Iowa State University, Ames, IA 50011, USA
6 Department of Anatomy, University of California San Francisco, San Francisco, CA 94143, USA

***Co-Corresponding Authors:** Anurag Das (anuragd7@iastate.edu), John P. Vaughen (john.vaughen@ucsf.edu), Hua Bai (hbai@iastate.edu)

Highlights

- Peroxisomal membrane and importer proteins are enriched in cortex glia (CG).
- The circadian clock autonomously decreases peroxisomal import in CG.
- The cytosolic importer Pex5 controls circadian peroxisomal import in CG.
- Loss of *Pex5* in CG disrupts brain lipid metabolism and sleep behavior.

Abstract

Peroxisomes are critical organelles that detoxify wastes while also catabolizing and anabolizing lipids. How peroxisomes coordinate protein import and support metabolic functions across complex tissues and timescales remains poorly understood *in vivo*. Using the *Drosophila* brain, we discover a striking enrichment of peroxisomes in the neuronal soma and the cortex glia that enwrap them. Unexpectedly, import of peroxisomal proteins into cortex glia, but not neurons, dramatically oscillated across time and peaked in the early morning. Rhythmic peroxisomal import in cortex glia autonomously required the circadian clock and Peroxin 5 (Pex5; peroxisomal biogenesis factor 5 homolog), with endogenous Pex5 protein peaking in the morning. Notably, removing *Pex5* in cortex glia severely reduced sleep while concomitantly causing aberrant lipid metabolism characterized by ectopic lipid droplets and increases across multiple lipid families. Thus, the circadian import of peroxisomal proteins via Pex5 in cortex glia is essential for lipid homeostasis and organismal behavior.

Key Words: Glia, circadian, metabolism, peroxisomes, Pex5, sleep homeostasis, lipid droplets, lipidomics, *Drosophila melanogaster*

Introduction

Peroxisomes are responsible for vital metabolic activities ranging from lipid metabolism by beta-oxidation and ether lipid biosynthesis[1,2,3] to reactive oxygen species detoxification[4,5 ,6]. Accordingly, mutations afflicting peroxisomes can cause numerous diseases, including Zellweger Syndrome[7,8], a severe peroxisomal biogenesis disorder stemming from mutations in one of the 12 different PEX genes in humans[9]. While these diseases often manifest in the brain[10,11,12] , how peroxisomes are regulated and function across diverse brain cells and timescales remains incompletely understood.

Intriguingly, peroxisomes require a unique import machinery capable of translocating fully folded and oligomeric substrates from the cytosol into the peroxisomal matrix (lumen)[13]. The Peroxin-5 protein Pex5 is a vital cog in this translocation machinery, as it functions as a major receptor for targeting proteins to the peroxisomal matrix by the peroxisomal targeting signal 1, or PTS1 (e.g. Ser-Lys-Leu)[14,15,16]. Notably, loss of Pex5 from *Drosophila* to mice and humans causes severe defects, including motor and cognitive decline simultaneously with demyelination, axonal loss, and gliosis[17]. While *Pex5* mutants are lethal[18], *Pex5* disruption selectively in mouse oligodendrocytes caused pronounced neurological and lipidomic defects[5]. In contrast, neuron or astrocyte *Pex5* disruption only led to mild defects[17]. While peroxisomal import may thus have cell-type specific effects in the brain, this has not been systematically explored across space and time *in vivo*.

Drosophila is an outstanding genetic model to interrogate how peroxisomes and peroxisomal import function in the brain, given the capability to genetically track and manipulate peroxisomal import in a cell-type specific manner. The fly brain harbors a diversity of glial subtypes and neurons though to share homologous functions with mammalian counterparts[19,20,21]. For example, neuronal soma are enwraped by glia similarly to satellite glia, while neuronal synaptic prcoesses are tiled by astrocyte-like glia and isolated and insulated by ensheathing (CNS)[22] and wrapping glia (PNS), analogous to schwann cells and oligodendrocytes[23]. Moreover, flies harbor complex behavioral repertoires ranging from memory to sleep and circadian biology[24,25,26,27,28] . Indeed, while all animal behavior is tightly coordinated by rhythmic changes experienced under the

109 shared 24-hour light/dark cycle[29,30] , in complex metazoan brains the clock is controlled
110 by a network of circadian pacemaker neurons and glia[31,32,33,34,35,36,37]. Circadian rhythms
111 govern metabolic homeostasis across organisms[38,39,40], yet their role in organelle
112 dynamics and peroxisome biology remains underexplored.
113
114 Here, we tested how peroxisomal import is spatiotemporally coordinated in the fly brain.
115 We discovered that specialized cortex glia are hubs of abundant matrix peroxisomal
116 proteins and high peroxisomal import, in contrast to other brain glia. Moreover,
117 peroxisomal import in cortex glia but not neurons varied dramatically over circadian time,
118 with a three-fold elevation of import in the early morning. Through genetic analyses, we
119 determined that Pex5 and the core circadian clock composing *Period* and *Clock* (*Bmal1*)
120 autonomously regulated the oscillatory peroxisomal import in cortex glia. Notably, loss of
121 Pex5 in cortex glia profoundly disrupted sleep behavior and brain lipid metabolism,
122 triggering the accumulation of ectopic lipid droplets and an overabundance of many lipid
123 species within the brain. Thus, circadian peroxisomal import restricted to specialized glia
124 is essential for brain-wide lipid metabolism and organismal sleep.
125
126
127
128 **Results**
129
130 **Peroxisomal abundance and import are enriched in neurons and cortex glia**

131 Peroxisomal import (Figure 1A) is the active translocation of matrix proteins from the
132 cytosol into the peroxisomal lumen via the canonical peroxisomal targeting signal 1
133 (PTS1; the commonest consensus tripeptide sequence is Serine-Lysine-Leucine, SKL).
134 These sequences are recognized by the cytosolic import receptor Pex5, which facilitates
135 shuttling by releasing imported cargo in the peroxisomal lumen[41,42]. We first sought to
136 survey peroxisome import in the adult CNS by co-staining for the peroxisomal marker
137 PMP70 (Peroxisomal membrane protein 70)[43,16,44,45] and *UAS-eYFP.PTS1*[46]*,* which
138 reveals cell-type specific patterns of peroxisome import when crossed to GAL4 driver
139 lines targeting major CNS populations (Figure 1B). Both pan-glial (*repo-GAL4*) and pan-

140 neuronal (*nSyb-GAL4*) drivers expressed PTS1 punctate that colocalized with PMP70
141 (Figure 1C). Notably, PMP70 was enriched at the cortex in pan-glial experiments,
142 suggesting that cortex glia may have particularly high levels of peroxisome import.
143 Indeed, by genetically tracking peroxisome import with *UAS-eYFP.PTS1* across different
144 glia subtypes, we found that PTS1+,PMP70+ punctate were most abundant in cortex glia
145 compared to other glia classes (Figure 1D-F; Figure S1A-D). Thus, among the CNS glia,
146 cortex glia have uniquely heightened peroxisomal import.

147 **Peroxisomal import oscillates in cortex glia across time and requires Pex5**

148 Cortex glia can encompass more than 50 neuronal cell bodies in a unique, honeycombed
149 morphology, and accordingly regulate neuronal activity among other functions
150 [20,19,47,48,49,50,51,22]. While further characterizing peroxisomal import in cortex glia, we made
151 the serendipitous finding that import fluctuated across circadian time in cortex glia but not
152 neurons (Figure 2A-B; Zeitgeber 0 (ZT0) denotes lights-on). While neurons had
153 consistently high levels of PTS1 that colocalized with PMP70, cortex glia had three-fold
154 higher levels of PTS1 at ZT2 compared to ZT8 (Figure 2C-F). A similar enrichment of
155 morning import was observed with an anti-SKL antibody (Figure S2B-D). While cortex glia
156 PTS1 puncta remained low in the evening, we noted that the colocalization between PTS1
157 and PMP70 at ZT14 was higher than at ZT8 (Figure 2C), and we often observed diffuse
158 PTS1 membranous signals at night at ZT14 (Figure S2E).
159
160 Intrigued, we tested whether the central regulator of peroxisomal import, Pex5 (Figure
161 1A), also oscillated in the brain. We used CRISPR to generate a knock-in FLAG tag into
162 the endogenous Pex5 locus (Figure 2G; Figure S2G and see Methods). *Pex5.FLAG* flies
163 were viable and healthy (Figure S2F-F'), unlike Pex5 loss-of-function alleles, which are
164 lethal[18]. Strikingly, the endogenous Pex5 protein robustly oscillated across time in the
165 brain, peaking at ZT2 during the height of PTS1 import in cortex glia (Figure 2H-I; Figure
166 S2A; note that the majority of Pex5 is expected to be cytosolic). Moreover, this oscillatory
167 signature is present in single cell RNA sequencing data, where transcripts of *Pex5*,
168 *Pex11*, and the PPAR homolog *Eip75B* peak at similar times in cortex glia[33] (Figure S3
169 A-B). To test if Pex5 is obligatory for basal levels of peroxisomal import in glia, we

170 knocked-down *Pex5* using *RNAi* in cortex glial and found strong suppression of overall
171 peroxisomal import, with reduced PTS1 puncta that no longer oscillated, but comparable
172 numbers of PMP70+ punctate (Figure 2J-M). Thus, in cortex glia, peroxisomal import and
173 Pex5 levels are highest in the morning, and oscillations in peroxisomal import require
174 Pex5.
175
176 **The circadian clock autonomously controls peroxisomal import in cortex glia**
177 To test if the circadian clock regulated peroxisomal import, we mutated *period* (*per*), an
178 essential transcription factor in the core circadian clock, and measured PTS1 import in
179 cortex glia at the apex (ZT2) and nadir (ZT8) of PTS1 import in cortex glia. Strikingly,
180 *period* mutants had persistently elevated PTS1 import in cortex glia (Figure 3A-E).
181 Additionally, removing the PPAR homolog and downstream target of Per, *Eip75B*, in
182 cortex glia phenocopied the effect of *per* and persistently elevated import (Figure S4A-
183 C). Lastly, as all glia and subsets of neurons express core circadian clock
184 machinery[52,53,54,55,56,33] , we investigated whether cortex glia autonomously require a
185 functioning circadian clock by leveraging a dominant-negative Clock transgene[57] (*UAS-*
186 *Clk*^{DN}). Indeed, autonomously expressing *Clk*^{DN} in cortex glia triggered aberrant and
187 persistently elevated levels of PMP70/SKL, phenocopying *period* and *Eip75B* (Figure 3F-
188 J). Thus, the circadian clock and Pex5 autonomously control rhythmic peroxisomal import
189 into a specialized subset of brain cells, the cortex glia, with import peaking early in the
190 morning and core-clock proteins mediating its rhythmic decline at ZT8.
191
192 **Loss of *Pex5* selectively in cortex glia disrupts sleep**
193
194 Given the striking circadian oscillations in peroxisomal import in cortex glia, and that
195 cortex glia regulate sleep behavior,[58,59] we next examined whether removing *Pex5* in
196 different cells altered sleep. Remarkably, disrupting *Pex5* in cortex glia halved daytime
197 sleep and reduced nighttime sleep by one-third (Figure 4A-A”), with shorter sleep bout
198 length but no overall changes in circadian rhythmicity (Figure S5A-B). In contrast,
199 knocking-down *Pex5* in ensheathing glia, which did not contain abundant PTS1+,
200 PMP70+ importing peroxisomes (Figure 1D), had no impact on daytime sleep and
201 inconsistent effects on nighttime sleep (Figure 4B-B”). Although neurons had high levels

202 of PTS1+,PMP70+ puncta, removing *Pex5* from neurons with *nSyb-GAL4* did not
203 consistently affect daytime or nighttime sleep (Figure 4C-C”). Thus, Pex5 plays a critical,
204 cell-type specific role in in cortex glial peroxisomal import that regulates sleep behavior.
205
206 **Cortex glial Pex5 is essential for lipid homeostasis in the adult brain**
207 Wakefulness causes accumulation of lipid droplets in cortex glia and ensheathing glia[59],
208 and peroxisomes can directly interact with lipid droplets (LD), with Pex5 stimulating
209 lipolysis[60,61]. We thus hypothesized that removing *Pex5* in cortex glia would alter LDs in
210 the brain. Indeed, knockdown of *Pex5* in cortex glia dramatically increased lipid droplet
211 number and size (Figure 5A-C), with lipid droplets adjacent to PMP70 puncta at the brain
212 cortex. Given these defects, and the known role of peroxisomes in lipid metabolism, we
213 profiled the brain lipidomes of cortex glia depleted of *Pex5* using liquid-chromatography
214 mass spectrometry (Figure 5D). While the overall distribution of most lipid families
215 remained similar between controls and $Pex5^{KD}$ brains (Figure 5E-F; Figure S6A),
216 numerous individual lipid species accumulated upon $Pex5^{KD}$ (Figure 5G), including
217 significant increases in glycerophospholipids, including phosphatidylcholines (PC) and
218 phosphatidylethanolamines (PE) (Figure 5H). Additionally, certain sphingolipid species
219 increased upon $Pex5^{KD}$ in cortex glia (Figure 5I), consistent with crosstalk between
220 peroxisomes and sphingolipid metabolism[62,63,3,64]. Intriguingly, many of these were d16
221 ceramide phosphoethanolamines (CPE) that are produced by neurons[65], suggesting
222 crosstalk between cortex glia and neuronal sphingolipid biosynthesis.
223
224 To further explore cell-type specific functions for Pex5 in regulating brain lipid metabolism,
225 we conducted pan-glial (*repo-GAL4*) and pan-neuronal (*nSyb-GAL4*) knockdowns of
226 *Pex5* and profiled brains at 8 days of age (Figure S6C). Similar to the loss of *Pex5* from
227 cortex glia, total lipid levels were unaffected, except for reduced triacylglycerols (TAG) in
228 glia knockdown brains. However, these stronger *Pex5* perturbations caused severe and
229 divergent alterations in glycerophospholipids, sphingolipids, and TAGs, as revealed by
230 principal component analysis and heatmaps (Figure S6D-E). Notably, pan-glial *Pex5*
231 knockdown had the strongest effects on PE and PC classes, accounting for ~50% of the
232 variance in PC1 (Figure S6D) and echoing the surprising effects of cortex glia *Pex5* on

233 these glycerophospholipids. While we did not detect increases in very long chain fatty
234 acids upon cortex glia knockdowns of *Pex5* (Figure S6B), C24.1 and C22.1 fatty acids
235 accumulated in either neuronal or pan-glial *Pex5* knockdown (Figure S6F).
236
237 Together, these data reveal that cortex glia require Pex5 for broadly regulating lipid
238 metabolism in the brain, and that loss of Pex5 in neurons or glia causes divergent deficits
239 in lipid metabolism.
240
241 **Discussion**
242
243 Here we uncover the novel circadian regulation of glial peroxisomal dynamics and link
244 clock-controlled organelle biology to brain-wide lipid metabolism and sleep behavior. By
245 systemic profiling of peroxisomal import in the brain, we elucidated that specialized cortex
246 glial have enriched and dynamic peroxisomal import early in the morning. The circadian
247 clock and Pex5 autonomously control circadian import into cortex glia, and cortex glia
248 Pex5 is essential for preventing lipid dysregulation and sleep loss.
249
250 ***An evolutionarily conserved role for Pex5 in glia***

251 Prior investigations discovered key roles for Pex5 in oligodendrocytes[5] and Schwann
252 cells[6], with severe neurodegeneration and demyelination in *Pex5* oligodendrocyte
253 knockouts, and nonautonomous effects on ion channel distribution downstream of
254 lysosomal dysfunction in Schwann cell knockouts. In contrast, knockout of *Pex5* in
255 neurons and astrocytes did not cause overt pathology[17]. By tracking peroxisomal import
256 and conducting *Pex5* knockout experiments across diverse brain cells, we found that
257 cortex glia are selectively enriched for Pex5-dependent circadian peroxisomal import.
258 Thus, in both flies and humans, glia play a central role in peroxisome-mediated
259 processes, and it would be exciting to test for circadian peroxisomal import in mammalian
260 glia which similarly enwrap neuronal soma. Homologues of the cortex glia based on
261 structural morphology include satellite glia cells, protoplasmic astrocytes, and
262 perineuronal oligodendrocytes[66,67,68,69]. Notably, cortex glia extend fine membrane
263 processes tiling over fifty neuronal cell soma, regulate neruonal activity[47,49], and serve as

264 reservoirs of energy and neutral lipids during development[70,51] and adulthood.[71] Due to
265 the close association of cortex glia with the neuronal cell soma, we speculate that
266 peroxisomes are vital to neuronal homeostasis through both lipid metabolic and cellular
267 detoxifying functions[72,73,47] . Indeed, the loss of *Pex5* in cortex glia lead to surprising
268 increases in many glycerophospholipids, paralleling increases in PE following *Pex5* loss
269 in oligodendrocytes that may compensate for decreased ether phospholipids[5]. Future
270 work should determine how circadian peroxisomal import by cortex glial acutely regulates
271 ether phospholipid and glycerophospholipid metabolism, and how this and other
272 peroxisomal functions could nonautonomously govern neuronal health.
273
274 ***Circadian control of peroxisomal import in cortex glia***
275
276 Circadian clocks regulate daily rhythms in organelle dynamics[38,74], lipid metabolites[75,76,77],
277 and transcriptomes in various tissues[78,79,80,81,82,83,84] . Our work raises the critical question
278 of how pervasively peroxisomal proteins and functions vary across circadian time. While
279 we demonstrate that Pex5 and peroxisomal import peak early in the morning at ZT2 and
280 have a trough at ZT8, future studies should test if all or subsets of peroxisomal proteins
281 are similarly circadian in cortex glia. Surprisingly, despite neurons containing high levels
282 of peroxisomal matric proteins and PTS1 puncta, we did not detect variations in import
283 across time. Why do cortex glia selectively enhance import in the morning? The circadian
284 clock mediated ZT8 afternoon cessation of peroxisomal import aligns well with the
285 concept of restorative breaks, as ZT8 entails the afternoon siesta thought to adjust for the
286 hottest time of the day[85]. These restorative breaks may be essential for clearing damaged
287 peroxisomes or for timing lipid metabolic loops, among other possible functions.
288
289 ***Pex5 as a central regulator of glial peroxisomes and organismal behavior***
290 Zellweger spectrum diseases[86,87] are a group of heterogenous mutations in peroxisomal
291 proteins that cause neurodevelopmental and neurodegenerative disorders.[88] As cortex
292 glial Pex5 is essential for sleep and subject to circadian regulation, it will be intriguing to
293 look for circadian modulation of Zellweger disorder phenotypes and sleep defects. Our
294 behavioral findings suggest that cortex glial communicate with closely associated

295 neuronal soma to intricately regulate behavioral processes such as sleep, which is driven
296 by complex interplays of neuronal circuits[89,90] . The sleep homeostat is tightly regulated
297 by a two-step regulatory process including circadian oscillations and homeostatic
298 regulation described in both humans and *Drosophila*[91,92] . While we link *period* and the
299 circadian clock to brain glial peroxisomal import, *period* mutant larval fat bodies have
300 ultradian variation in lipid metabolism and peroxisomal import and biogenesis[93],
301 suggesting there may be both clock and non-clock based mechanisms at play.
302 Intriguingly, a putative deubiquitinase for Pex5, USP2, shows circadian fluctuations in
303 localization to the peroxisome in liver that depends on the core clock[94], and a similar
304 mechanism may regulate the stability and activity of Pex5 in the cortex glia.

305 The association of Period with peroxisomal import regulation in brain glia could provide
306 insight into age associated sleep disorders. Indeed, sleep deprivation induces a cytokine
307 storm[95], and *Pex5* perturbation induce pro-inflammatory cytokine *upd3* in glial cells[4]. In
308 flies, altered lipid droplet metabolism in cortex and ensheathing glia downstream of
309 neuronal oxidative stress can cause sleep defects[59]**.** Given that *Pex5* knockdown in
310 cortex glia caused sleep loss and increased lipid droplets, we speculate that neurons in
311 aged $Pex5^{KD}$ flies could accumulate reactive oxygen species and upregulated cytokines
312 through neuronal-glia crosstalk, and that our observations of increased lipid droplets may
313 reflect this metabolic coupling between neurons and glia.

314 Our identification of circadian import in cortex glia for sleep opens the avenue to a deeper
315 understanding of the spatiotemporal segregation of organelle function in the brain, and
316 the neurological consequences of peroxisomal disorders.

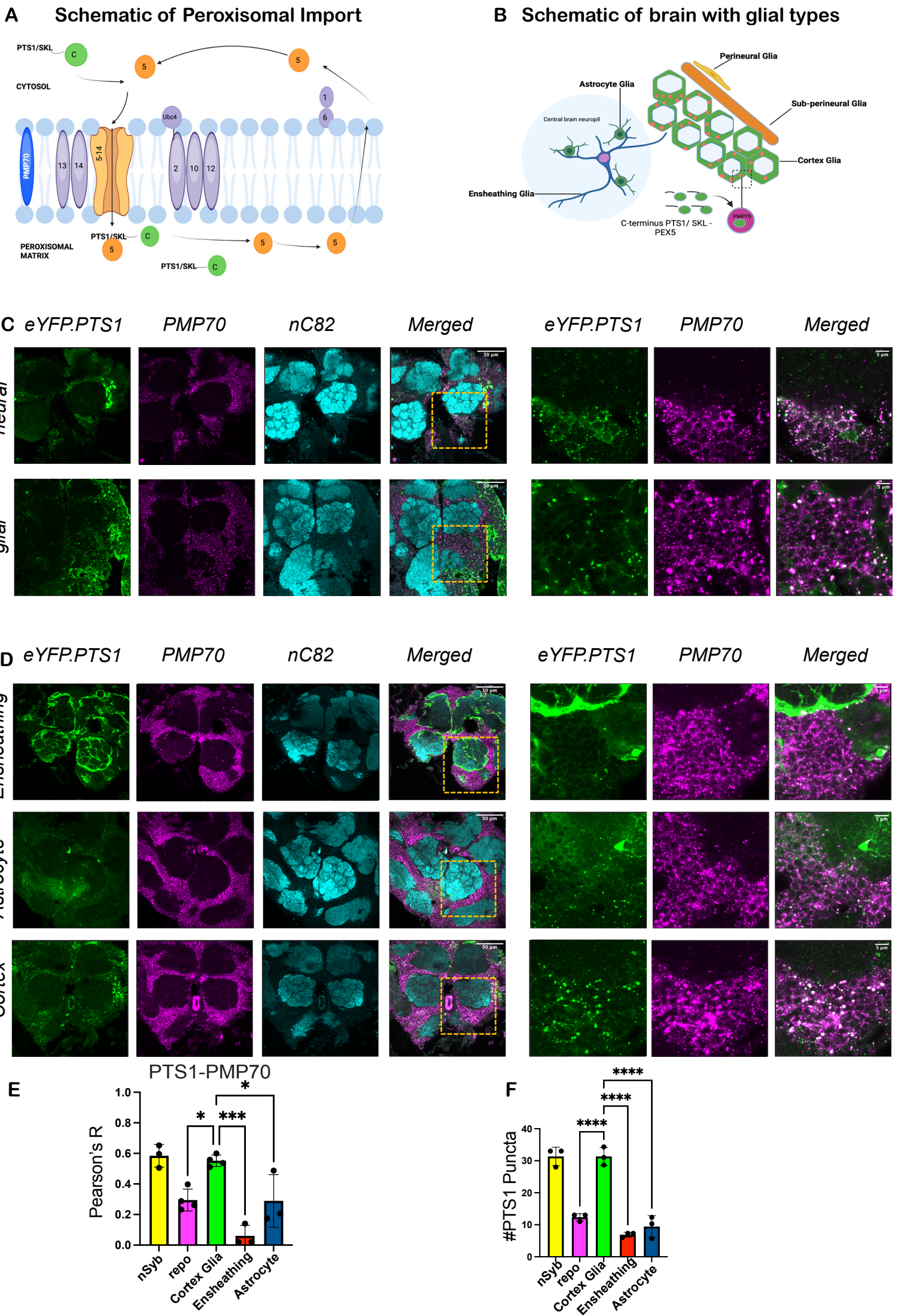
A Schematic of Peroxisomal Import
PTS1/SKL
C
5
5
CYTOSOL
1
6
Ubc4
PMP70
13
14
5-14
2
10
12
PTS1/SKL
C
5
5
5
PEROXISOMAL MATRIX
PTS1/SKL
C
B Schematic of brain with glial types
Perineural Glia
Astrocyte Glia
Sub-perineural Glia
Central brain neuropil
Cortex Glia
Ensheathing Glia
C-terminus PTS1/ SKL - PEX5
PMP70
C eYFP.PTS1 PMP70 nC82 Merged eYFP.PTS1 PMP70 Merged
neural
glial
D eYFP.PTS1 PMP70 nC82 Merged eYFP.PTS1 PMP70 Merged
Ensheathing
Astrocyte
Cortex
E
PTS1-PMP70
Pearson's R
1.0
0.8
0.6
0.4
0.2
0.0
*
***
*
nSyb
repo
Cortex Glia
Ensheathing
Astrocyte
F
#PTS1 Puncta
40
30
20
10
0
****
****
****
nSyb
repo
Cortex Glia
Ensheathing
Astrocyte

Figure 1. Peroxisomal abundance and import are enriched in neurons and cortex glia

(A) Schema of peroxisomal import machinery mediated by Pex5, the cytosolic import receptor that recognizes a *PTS1-SKL* harboring matrix protein and permits its active translocation from the cytosol to the peroxisomal lumen; Adapted from *Smith & Aitchison 2013; Skowyra et al., 2024*.

(B) Schematic of different glial cell types in the *Drosophila* central nervous system.

(C) Adult female *Drosophila* brains (7 days old) tracking peroxisome import in neurons with *UAS-eYFP.PTS1* using the pan-neural driver *nSyb-GAL4* or the pan-glial driver *repo-GAL4*. eYFP-tagged *PTS1*-protein import (green) is counterstained with PMP70 (magenta), an abundant peroxisomal membrane protein, and the pre-synaptic active zone protein bruchpilot (cyan; nc82). Yellow rectangle denotes area used for zooms into cortex. Scale bars = 50µm and 5µm (zoom).

(D) Adult female *Drosophila* brains (7 days old) tracking peroxisomal import in glia subtypes using *UAS-eYFP.PTS1* (green) driven by *GMR56F03*-GAL4 (Ensheathing glia), *GMR83E10-GAL4* (Astrocyte-like glia), and cortex glia (*GMR54H02*-GAL4), counterstained with PMP70 (magenta) and nc82 (cyan). Yellow rectangle denotes area used for zooms into cortex. Scale bars = 50µm and 5µm (zoom).

(E) Quantification of PTS1-YFP and PMP70 Pearson colocalization across different cellular populations. $n \geq 3$ brains per genotype, data points represent biological replicates averaged over ≥ 3 ROIs.

(F) Quantification of the number of PTS1-YFP punctate across different cellular populations. $n \geq 3$ brains per genotype, dots represent biological replicates averaged over ≥ 3 ROIs.

* $p < 0.05$, ** $p < 0.01$, *** $p < 0.001$, **** $p < 0.0001$ by Šídák's multiple comparisons test.

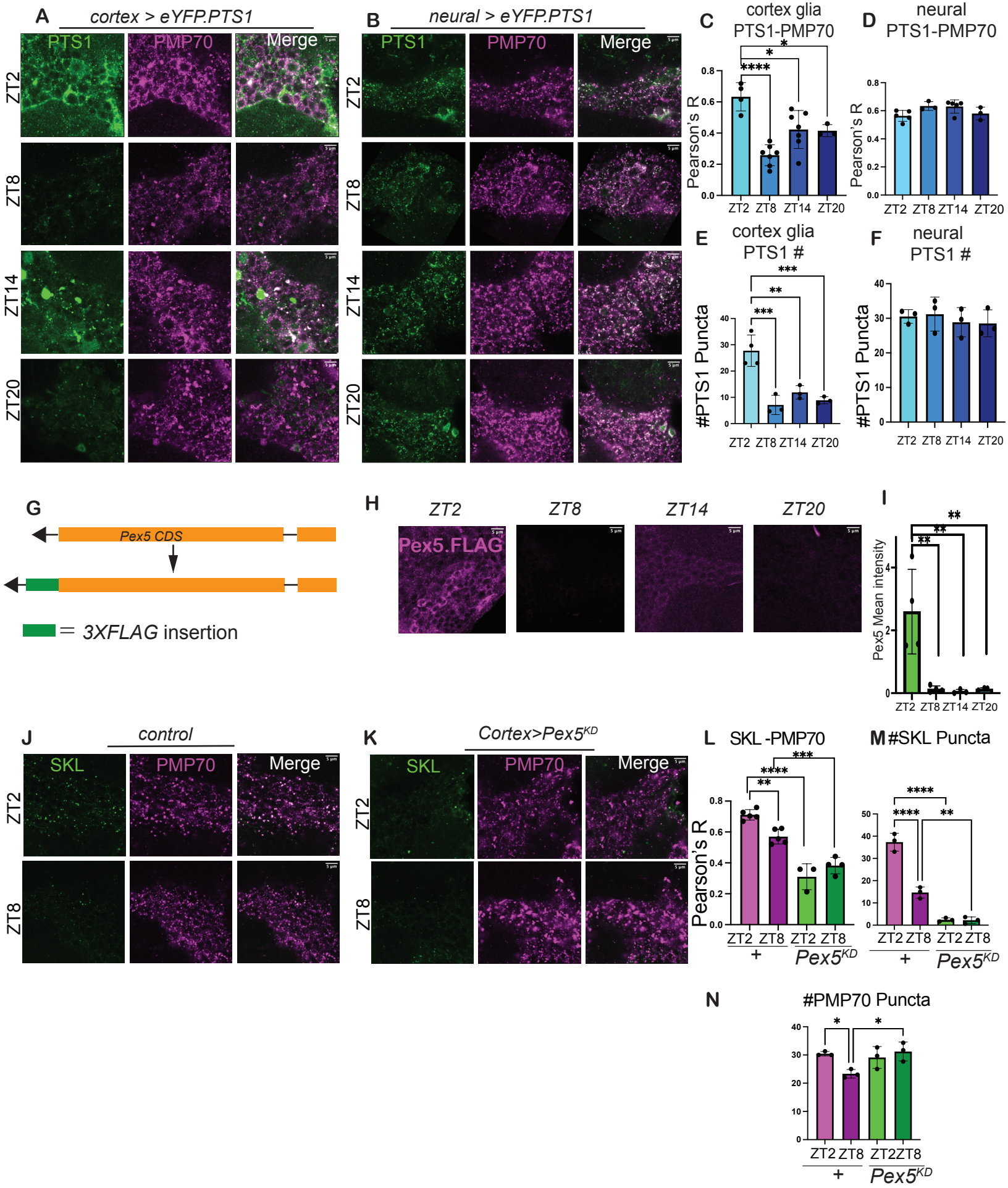
A
cortex > eYFP.PTS1
PTS1
PMP70
Merge
ZT2
ZT8
ZT14
ZT20
B
neural > eYFP.PTS1
C
cortex glia
PTS1-PMP70
Pearson's R
D
neural
PTS1-PMP70
E
cortex glia
PTS1 #
#PTS1 Puncta
F
neural
PTS1 #
G
Pex5 CDS
= 3XFLAG insertion
H
ZT2
ZT8
ZT14
ZT20
Pex5.FLAG
I
Pex5 Mean intensity
J
control
SKL
K
Cortex>Pex5KD
L
SKL -PMP70
M
#SKL Puncta
N
#PMP70 Puncta
+
Pex5KD

Figure 2. Peroxisomal import oscillates in cortex glia across time and requires *Pex5*

(A) Adult female *Drosophila* brains (7 days old) tracking peroxisomal import oscillation across ZT2, ZT8, ZT14, and ZT20 in cortex glia with *UAS-eYFP.PTS1* crossed to *GMR54H02-GAL4*. eYFP-tagged *PTS1*-protein import (green) is counterstained with PMP70 (magenta), an abundant peroxisomal membrane protein. Scale bars = 5µm.

(B) Adult female *Drosophila* brains (7 days old) tracking peroxisomal import oscillation across ZT2, ZT8, ZT14, and ZT20 in neurons with *UAS-eYFP.PTS1* crossed to the pan-neural driver *nSyb-GAL4.* eYFP-tagged *PTS1*-protein import (green) is counterstained with PMP70 (magenta), an abundant peroxisomal membrane protein. Scale bars = 5µm.

(C) Quantification of PTS1-YFP and PMP70 Pearson colocalization across cortex glia. *n* ≥*3* brains per genotype, data points represent biological replicates averaged over ≥*3* ROIs.
(D) Quantification of PTS1-YFP and PMP70 Pearson colocalization across neurons. *n* ≥*3* brains per genotype, data points represent biological replicates averaged over ≥*3* ROIs.
(E) Quantification of the number of PTS1-YFP punctate across cortex glia. *n* ≥*3* brains per genotype, dots represent biological replicates averaged over ≥*3* ROIs.
(F) Quantification of the number of PTS1-YFP punctate across neurons. *n* ≥*3* brains per genotype, dots represent biological replicates averaged over ≥*3* ROIs.

(G) Schema of *Pex5.FLAG* knock-in generated using CRISPR/Cas9-mediated gene editing in *Drosophila*.
(H) Adult female *Drosophila* brains (7 days old) tracking *Pex5.FLAG* knock-in stained with *anti-FLAG* (magenta) across ZT2, ZT8, ZT14, and ZT20.
(I) Quantification of the number of Pex5 mean intensity. *n* ≥*3* brains per genotype, dots represent biological replicates.

(J) Adult female *Drosophila* brains (7 days old) stained with SKL (green) and PMP70 (magenta) in control *UAS-Pex5 RNAi>w^{1118}.*

(K) Adult female *Drosophila* brains (7 days old) stained with SKL (green) and PMP70 (magenta) in cortex-glia specific knockdown of Pex5 using *GMR54H02-Gal4> UAS-Pex5 RNAi.*

(L) Quantification of PTS1-YFP and PMP70 Pearson colocalization. *n* ≥*3* brains per genotype, data points represent biological replicates averaged over ≥*3* ROIs.
(M) Quantification of the number of SKL punctate. *n* ≥*3* brains per genotype, dots represent biological replicates averaged over ≥*3* ROIs.
(N) Quantification of the number of PMP70 punctate. *n* ≥*3* brains per genotype, dots represent biological replicates averaged over ≥*3* ROIs.

* $p < 0.05$, ** $p < 0.01$, *** $p < 0.001$, **** $p < 0.0001$ by Tukey's multiple comparisons test.

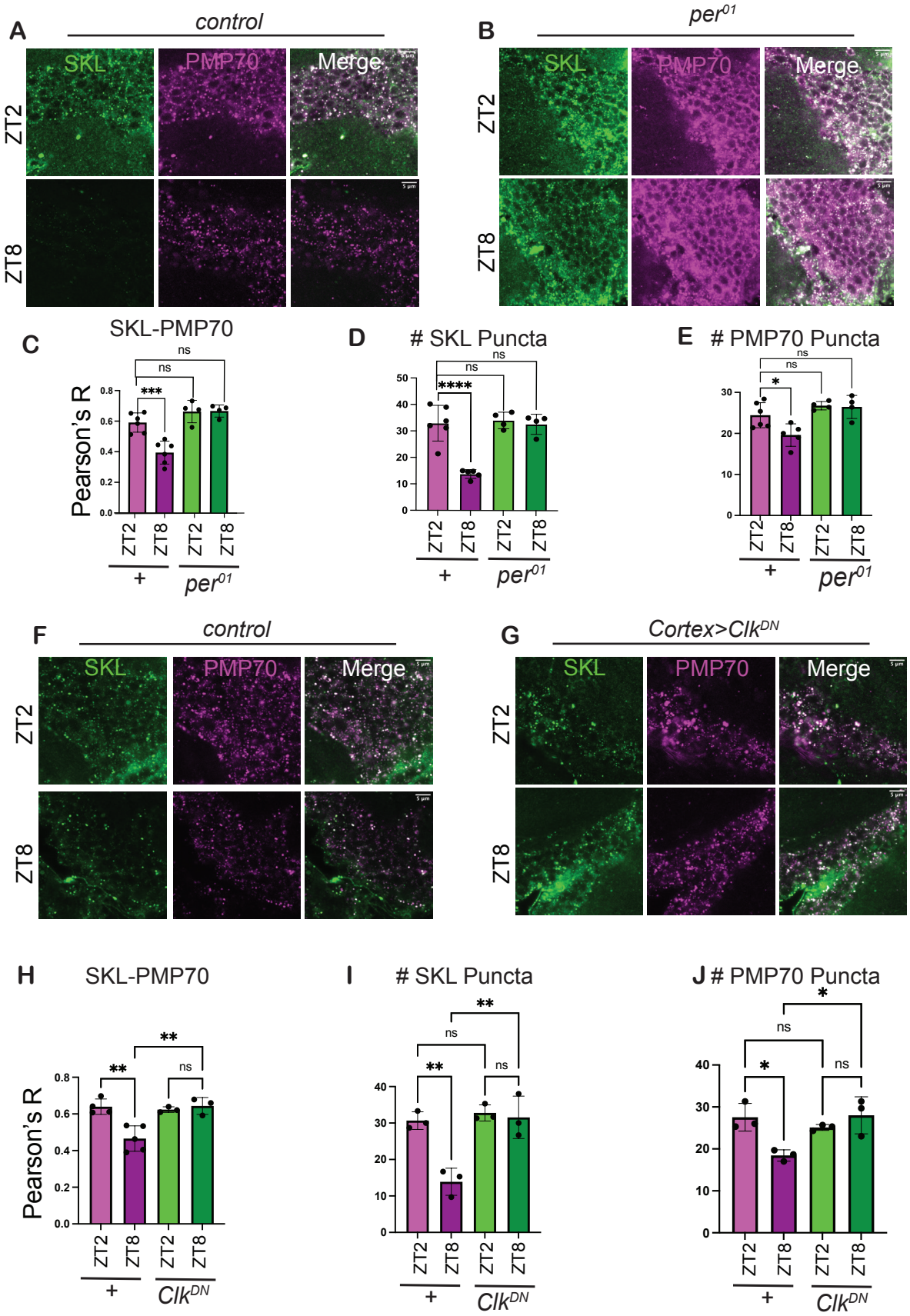
A
control
SKL
PMP70
Merge
ZT2
ZT8
B
per01
C
SKL-PMP70
Pearson's R
ns
***
+
per01
D
SKL Puncta
****
E
PMP70 Puncta
*
F
control
G
Cortex>ClkDN
H
SKL-PMP70
**
ClkDN
I
SKL Puncta
J
PMP70 Puncta

Figure 3. The circadian clock autonomously controls peroxisomal import in cortex glia

(A) Adult female *Drosophila* brains (7 days old) tracking peroxisomal import oscillation across ZT2, ZT8 in Control – *CantonS* with SKL (green) counterstained with PMP70 (magenta).

(B) Adult female *Drosophila* brains (7 days old) tracking peroxisomal import oscillation across ZT2, ZT8 in clock mutant - *Per[01]* with SKL (green) counterstained with PMP70 (magenta).

(C) Quantification of PTS1-YFP and PMP70 Pearson colocalization. *n ≥3* brains per genotype, data points represent biological replicates averaged over ≥*3* ROIs.

(D) Quantification of the number of SKL punctate. *n ≥3* brains per genotype, dots represent biological replicates averaged over ≥*3* ROIs.

(E) Quantification of the number of PMP70 punctate. *n ≥3* brains per genotype, dots represent biological replicates averaged over ≥*3* ROIs.

(F*)* Adult female *Drosophila* brains (7 days old) stained with SKL (green) and PMP70 (magenta) in UAS-control - *UAS-CLK-DN> w^{1118}.*

(G) Adult female *Drosophila* brains (7 days old) stained with SKL (green) and PMP70 (magenta) in Cortex-Glia>*UAS-Clk-Dominant negative(DN) – GMR54H04-Gal4>UAS-CLK-DN.*

(H) Quantification of PTS1-YFP and PMP70 Pearson colocalization. *n ≥3* brains per genotype, data points represent biological replicates averaged over ≥*3* ROIs.

(I) Quantification of the number of SKL punctate. *n ≥3* brains per genotype, dots represent biological replicates averaged over ≥*3* ROIs.

(J) Quantification of the number of PMP70 punctate. *n ≥3* brains per genotype, dots represent biological replicates averaged over ≥*3* ROIs.

ns – non-significant, * $p < 0.05$, ** $p < 0.01$, *** $p < 0.001$, **** $p < 0.0001$ by Tukey's multiple comparisons test.

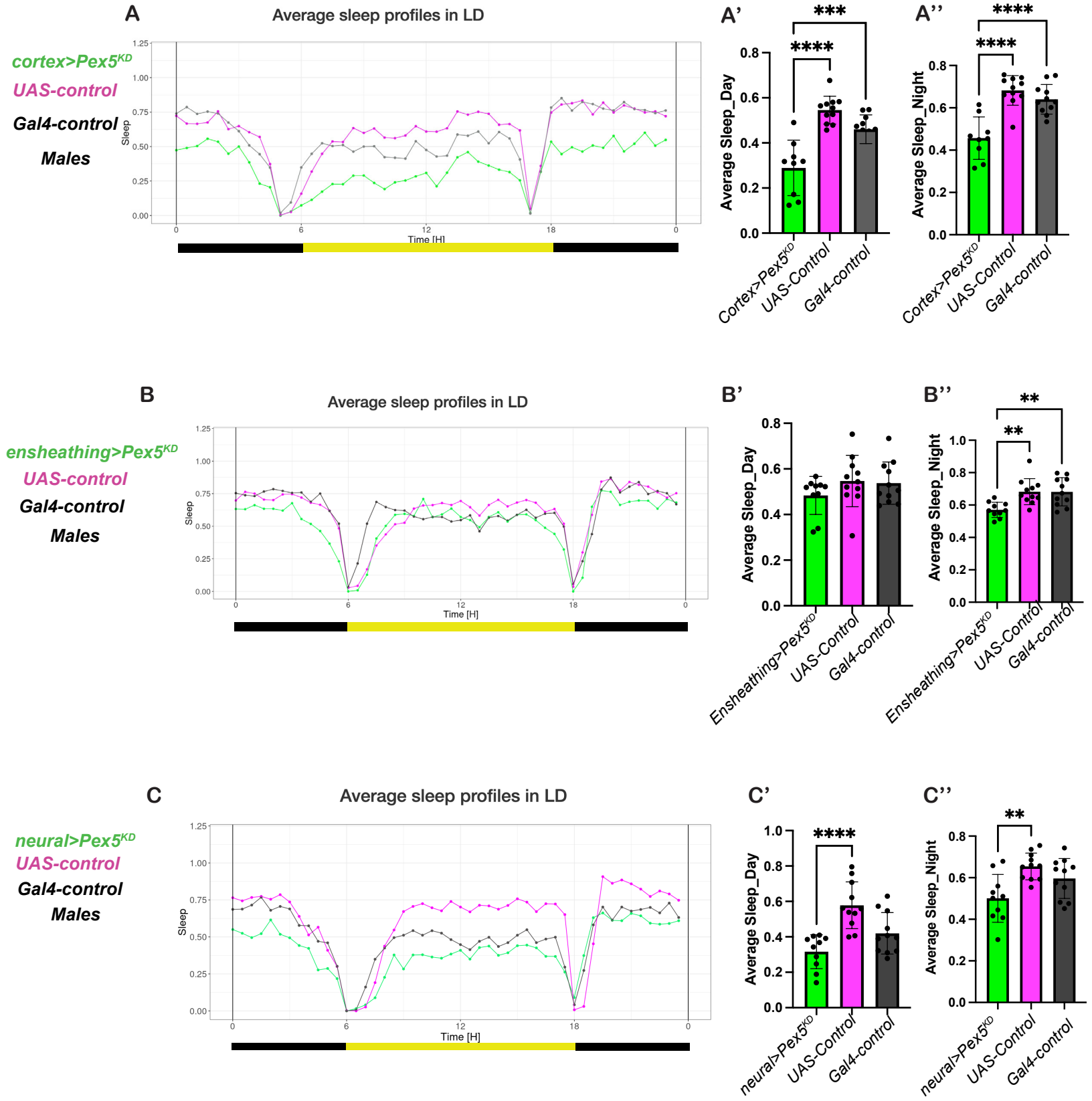
A
Average sleep profiles in LD
cortex>Pex5KD
UAS-control
Gal4-control
Males
Sleep
Time [H]
A'
A''
Average Sleep_Day
Average Sleep_Night
Cortex>Pex5KD
UAS-Control
Gal4-control
B
Average sleep profiles in LD
ensheathing>Pex5KD
UAS-control
Gal4-control
Males
B'
B''
Ensheathing>Pex5KD
C
Average sleep profiles in LD
neural>Pex5KD
UAS-control
Gal4-control
Males
C'
C''
neural>Pex5KD

Figure 4. Loss of *Pex5* selectively in cortex glia disrupts sleep

(A) Sleep was measured for 12hr/12hr, light/dark cycle on an average for 4-5 days continuously for 5-day to 10-day old males. Average circadian time-plot showing percent sleeping (bouts of inactivity > 5 mins) for the cortex glia driver *GMR77A03-GAL4* crossed with *UAS-Pex5 RNAi* (green) compared to parental controls (*UAS-Pex5-RNAi,* magenta *& GMR77A03-GAL4,* charcoal*)*.
(A') Daytime sleep quantified for genotypes from A. Individual black dots represent different biological replicates.
(A'') Night-time sleep quantified for genotypes from A.

(B) Sleep was measured for 12hr/12hr, light/dark cycle on an average for 4-5 days continuously for 5-day to 10-day old males. Average circadian time-plot showing percent sleeping for the ensheathing glia driver *GMR56F03-GAL4* crossed with *UAS-Pex5 RNAi* (green) compared to parental controls (*UAS-Pex5-RNAi,* magenta *& GMR56F03-GAL4,* charcoal*)*.
(B') Daytime sleep quantified for genotypes from B. Individual black dots represent different biological replicates.
(B'') Night-time sleep quantified for genotypes from B.

(C) Sleep was measured for 12hr/12hr, light/dark cycle on an average for 4-5 days continuously for 5-day to 10-day old males. Average circadian time-plot showing percent sleeping for the neuronal driver *nSyb-GAL4* crossed with *UAS-Pex5 RNAi* (green) compared to parental controls (*UAS-Pex5-RNAi,* magenta *& nSyb-GAL4,* charcoal*)*.
(C') Daytime sleep quantified for genotypes from C. Individual black dots represent different biological replicates.
(C'') Night-time sleep quantified for genotypes from C.

* $p < 0.05$, ** $p < 0.01$, *** $p < 0.001$, **** $p < 0.0001$ by Tukey's multiple comparisons test.

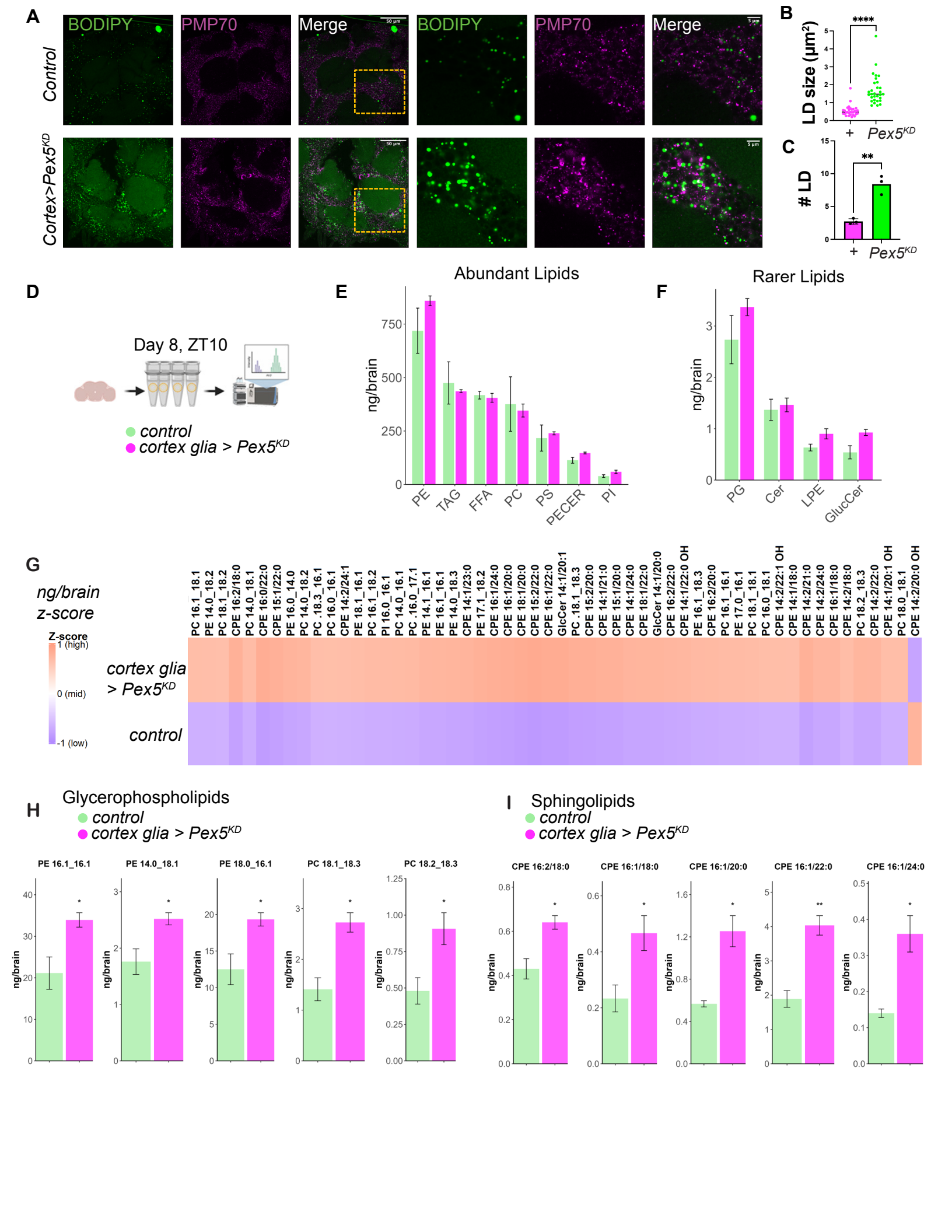
A
BODIPY
PMP70
Merge
Control
Cortex>Pex5KD
B
LD size (µm²)
****
+
Pex5KD
C
LD
**
D
Day 8, ZT10
control
cortex glia > Pex5KD
E
Abundant Lipids
ng/brain
PE
TAG
FFA
PC
PS
PECER
PI
F
Rarer Lipids
PG
Cer
LPE
GlucCer
G
ng/brain
z-score
Z-score
1 (high)
0 (mid)
-1 (low)
cortex glia > Pex5KD
control
H
Glycerophospholipids
control
cortex glia > Pex5KD
PE 16.1_16.1
PE 14.0_18.1
PE 18.0_16.1
PC 18.1_18.3
PC 18.2_18.3
I
Sphingolipids
control
cortex glia > Pex5KD
CPE 16:2/18:0
CPE 16:1/18:0
CPE 16:1/20:0
CPE 16:1/22:0
CPE 16:1/24:0

Figure 5. Cortex glial Pex5 is essential for lipid homeostasis in the adult brain.

(A) Adult female *Drosophila* brains (7 days old) tracking neutral lipid droplet (BODIPY 493/503, green) counterstained with PMP70 (magenta). Representative images of UAS-control (*UAS-Pex5 RNAi>w^{1118}*) versus cortex-glia specific knockdown of Pex5 using *GMR54H02-Gal4>UAS-Pex5 RNAi*.

(B) Quantification of different lipid droplet size(um^2) from A.
n ≥*3* brains per genotype, dots represent individual lipid droplets per biological replicates averaged over ≥*3* ROIs.

(C) Quantification of lipid droplet count from A. *n* ≥*3* brains per genotype, dots represent number of lipid droplets per biological replicates averaged over ≥*3* ROIs.

(A) Schematic workflow for control and *Cortex glia>Pex5^{KD}* (day8, ZT10) for lipidomics of dissected brains.

(B) Abundant lipids compared between controls (green) and *Cortex glia>Pex5^{KD}* (magenta)

(C) Rarer lipids compared between controls (green) and *Cortex glia>Pex5^{KD}* (magenta)

(D) Heat map of z-scored lipid species using ng/brain abundance in control vs *Cortex glia>Pex5^{KD}*

(E) Bar plots of major glycerophospholipids that increase upon *Pex5^{KD}* (magenta).
(F) Bar plots of major sphingolipids that increase upon *Pex5^{KD}* (magenta).

* $p < 0.05$, ** $p < 0.01$, *** $p < 0.001$, **** $p < 0.0001$ by Tukey's multiple comparisons test.

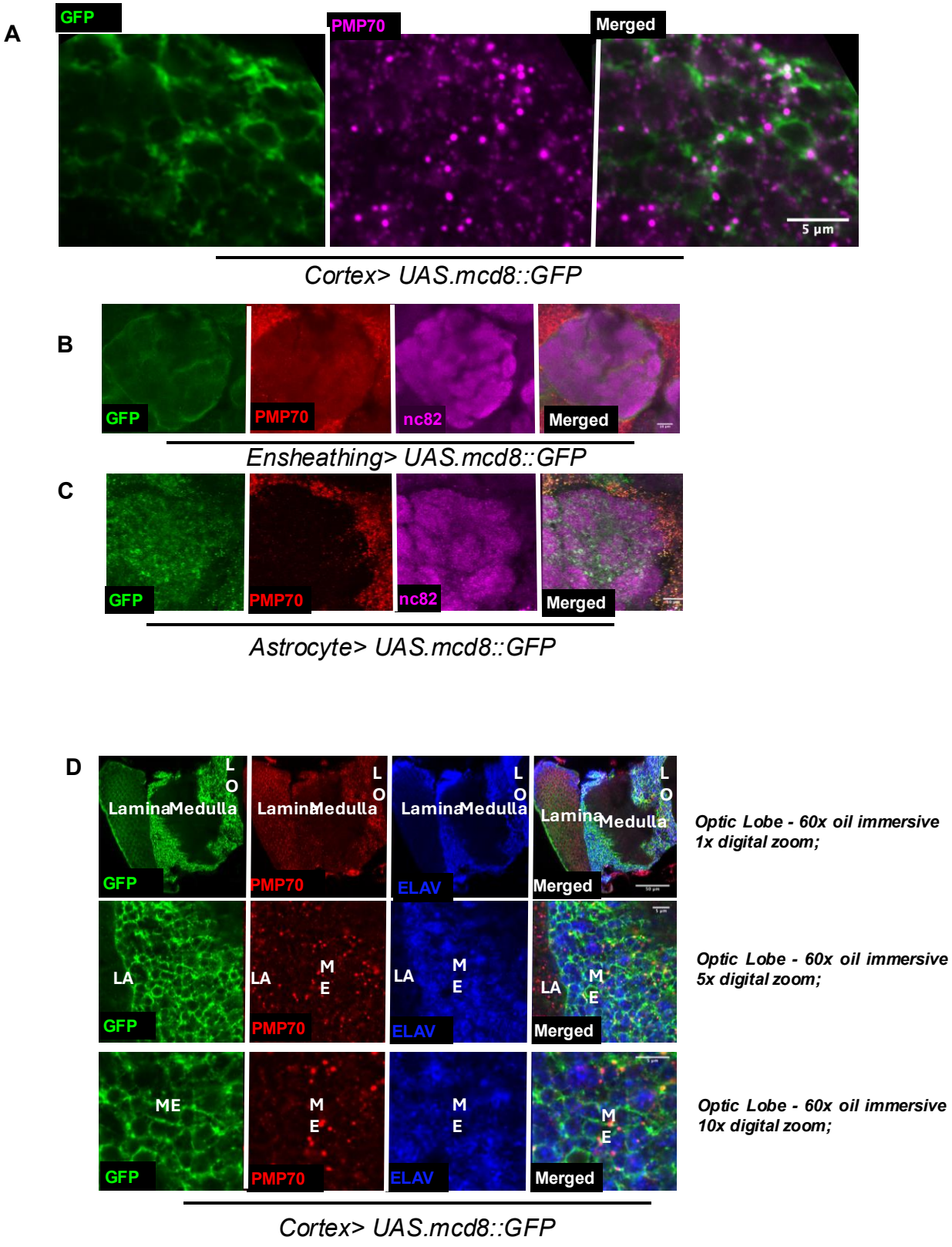

Figure 1 Supplemental

Figure S1, related to Figure1 -Representative images comparing central brain enriched glial classes – colocalization between GFP(green) counterstained with *PMP70(magenta)*. Thus, denoting the specificity of PMP70 peroxisomes in the glial cell to the regions of cortex glia showing its abundance compared to Ensheathing and astrocytic glia; nC82(magenta) marks the pre-synaptic active zones representing the neuropils of the adult *Drosophila* brain.

(A) Adult female *Drosophila* brains (7 days old) Cortex glia – *GMR54H02*-GAL4> UAS-*mCD8::GFP* tracking colocalization between GFP(green) counterstained with PMP70(magenta).

(B) Adult female *Drosophila* brains (7 days old) Ensheathing glia - *GMR56F03*-GAL4> UAS-*mCD8::GFP* tracking colocalization between GFP(green) counterstained with PMP70(red) and nc82 (magenta).

(C) Adult female *Drosophila* brains (7 days old) astrocytic glia – *alrm*-GAL4> UAS-*mCD8::GFP* tracking colocalization between GFP(green) counterstained with PMP70(red) and nc82 (magenta).

D) Adult female *Drosophila* brains (7 days old) Cortex glia – *GMR54H02*-GAL4> UAS-*mCD8::GFP* representative image showing the optic lobe regions (LA-lamina; ME-medulla; LO-lobula) showing conserved colocalization of PMP70 (red) positive puncta in GFP(green) rich regions of cortex glial; ELAV (blue) represents the neuronal cell body where no *PMP70*-positive (red) puncta is observed showing the high specificity of the peroxisomes to the cortex glial regions only.

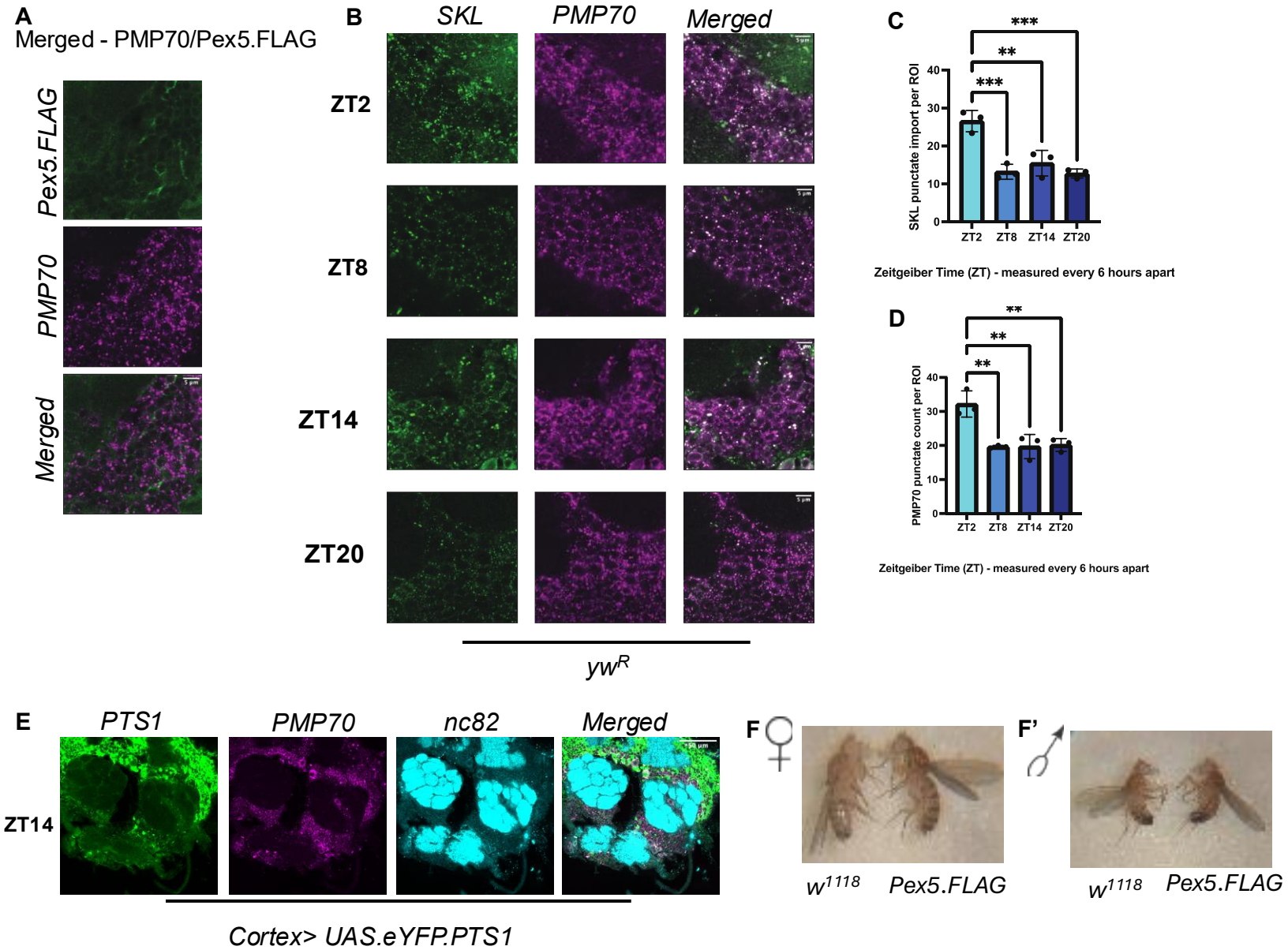

G

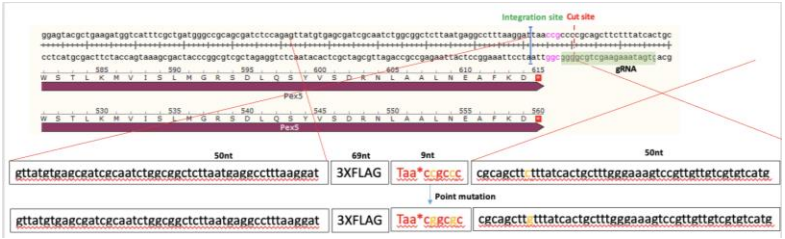

Figure 2- Supplemental

Figure S2, related to Figure 2.

(A) Adult female *Drosophila* brains (7 days old) tracking Pex5.FLAG Knock-in flies co-stained with anti-FLAG(green) and anti-PMP70(magenta).

(B) Adult female *Drosophila* brains (7 days old) yw^R wildtype flies dissected across ZT2, ZT8, ZT14 and ZT20 and stained with anti-SKL(green), anti-PMP70(magenta) to show circadian oscillations of peroxisomal import peak at ZT2 and trough at ZT8.

(C) Quantification in yw^R wildtype flies of *SKL* puncta at ZT2, ZT8, ZT14, ZT20. $n \geq 3$ brains per genotype, dots represent biological replicates averaged over ≥ 3 ROIs.

(D) Quantification in yw^R wildtype flies of PMP70 puncta at ZT2, ZT8, ZT14, ZT20;

(E) Adult female *Drosophila* brains (7 days old) tracking peroxisomal import oscillation at ZT14 observed in glia with *UAS-eYFP.PTS1* using *GMR54H02-gal4*, cortex glia specific gal4. eYFP-tagged *PTS1*-protein import (green) is counterstained with PMP70 (magenta), an abundant peroxisomal membrane protein to detect peroxisomes along with *anti-nc82*. Scale bar = 50µm.

(F) Adult female *Drosophila* comparing w^{1118} V/S *Pex5.FLAG.*

(F') Adult male *Drosophila* comparing w^{1118} V/S *Pex5.FLAG.*

(G) CRISPR/Cas9-based knock-in strategy to tag *Pex5* with a 3XFLAG epitope.

* $p < 0.05$, ** $p < 0.01$, *** $p < 0.001$, **** $p < 0.0001$ by Šídák's multiple comparisons test.

A

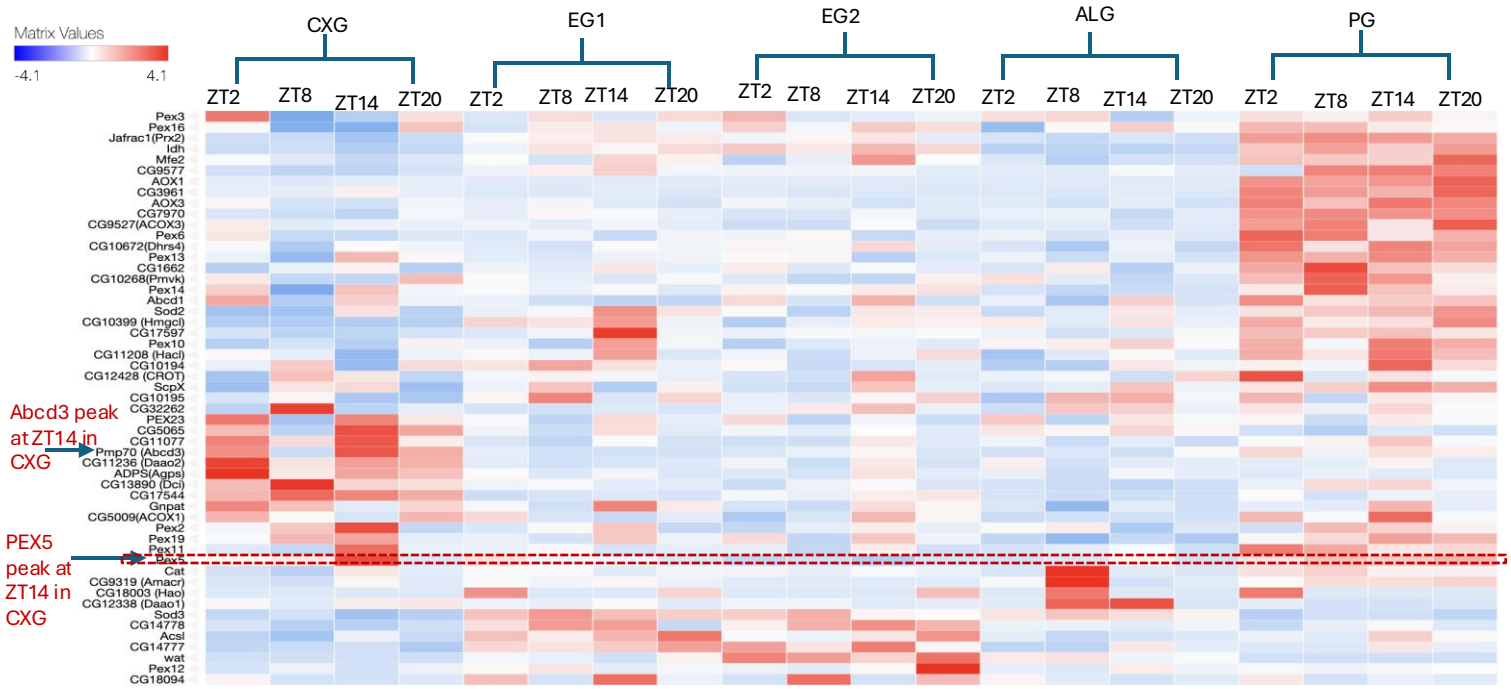

Global Heat map of peroxisomal differentially expressed genes in glial clusters at different ZT (zeitgeber) time points from Drosophila sleep single-cell

B

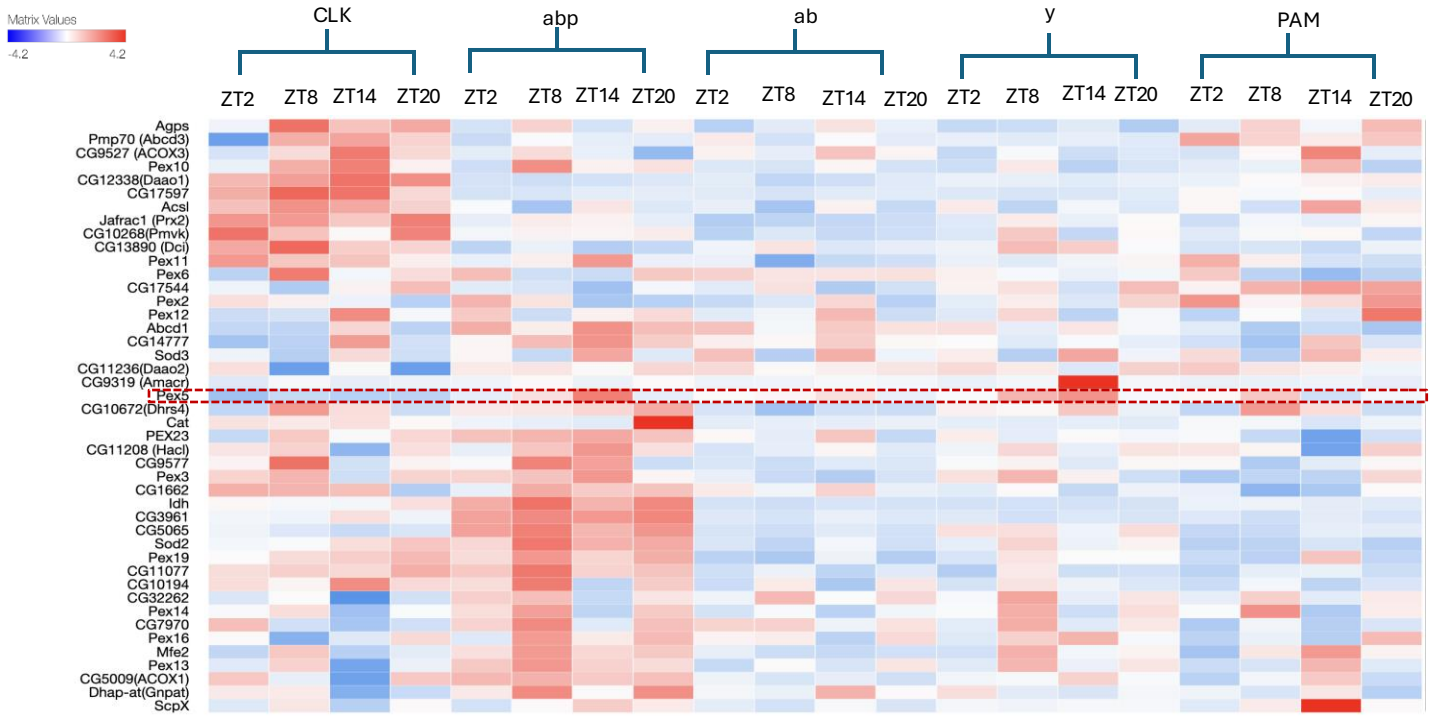

Global Heat map of peroxisomal differentially expressed genes in Neuronal clusters from Drosophila sleep single-cell

Figure 3- Supplemental

Figure S3, related to Figure 2.
(A) Global heatmap of peroxisomal gene expression extracted from fly-sleep single across all glial clusters to show *Pex5* expression is highest in CXG *(*cortex-glia) cluster.

(B) Global heatmap of peroxisomal gene expression extracted from fly-sleep single across neuronal clusters to show low *Pex5* expression as opposed to CXG glial cluster.

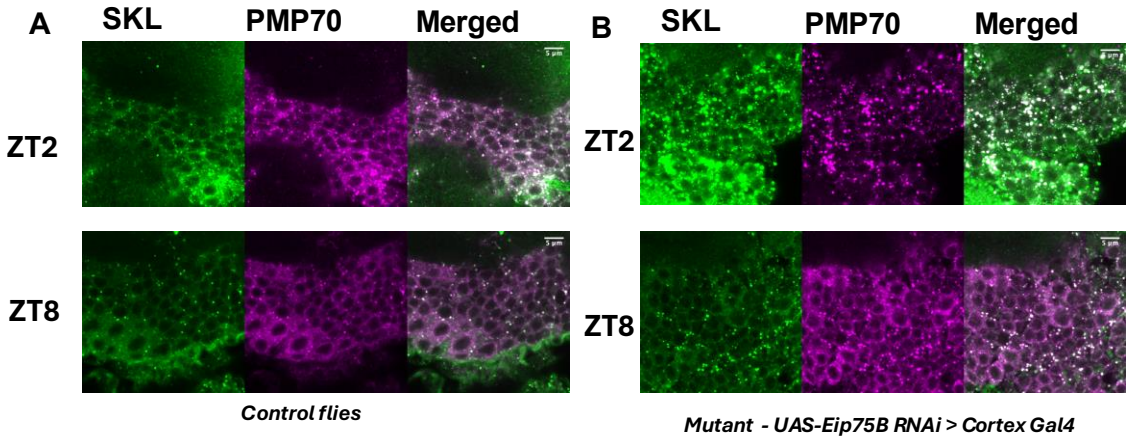

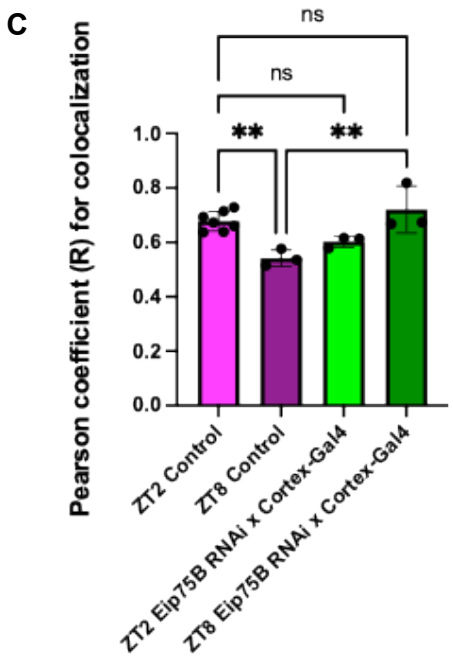

Figure 4- Supplemental

Figure S4, related to Figure 3.
(A) Adult female *Drosophila* brains (7 days old) dissected at ZT2 & ZT8 for control flies - *UAS-Eip75B* RNAi> w^{1118} stained with *anti-SKL(green)* and *anti-PMP70(magenta).*

(B) Adult female *Drosophila* brains (7 days old) dissected at ZT2 & ZT8 for *GMR54H02-Gal4>UAS-Eip75B* RNAi knockdown flies.

(C) Quantification Pearson R coefficient colocalization calculated (see methods) for *GMR54H02-Gal4* cross with *UAS-Eip75B* RNAi knockdown flies compared with control flies at ZT2, ZT8; $n \geq 3$ brains per genotype, dots represent biological replicates averaged over ≥ 3 ROIs.

* $p < 0.05$, ** $p < 0.01$, *** $p < 0.001$, **** $p < 0.0001$ by Šídák's multiple comparisons test.

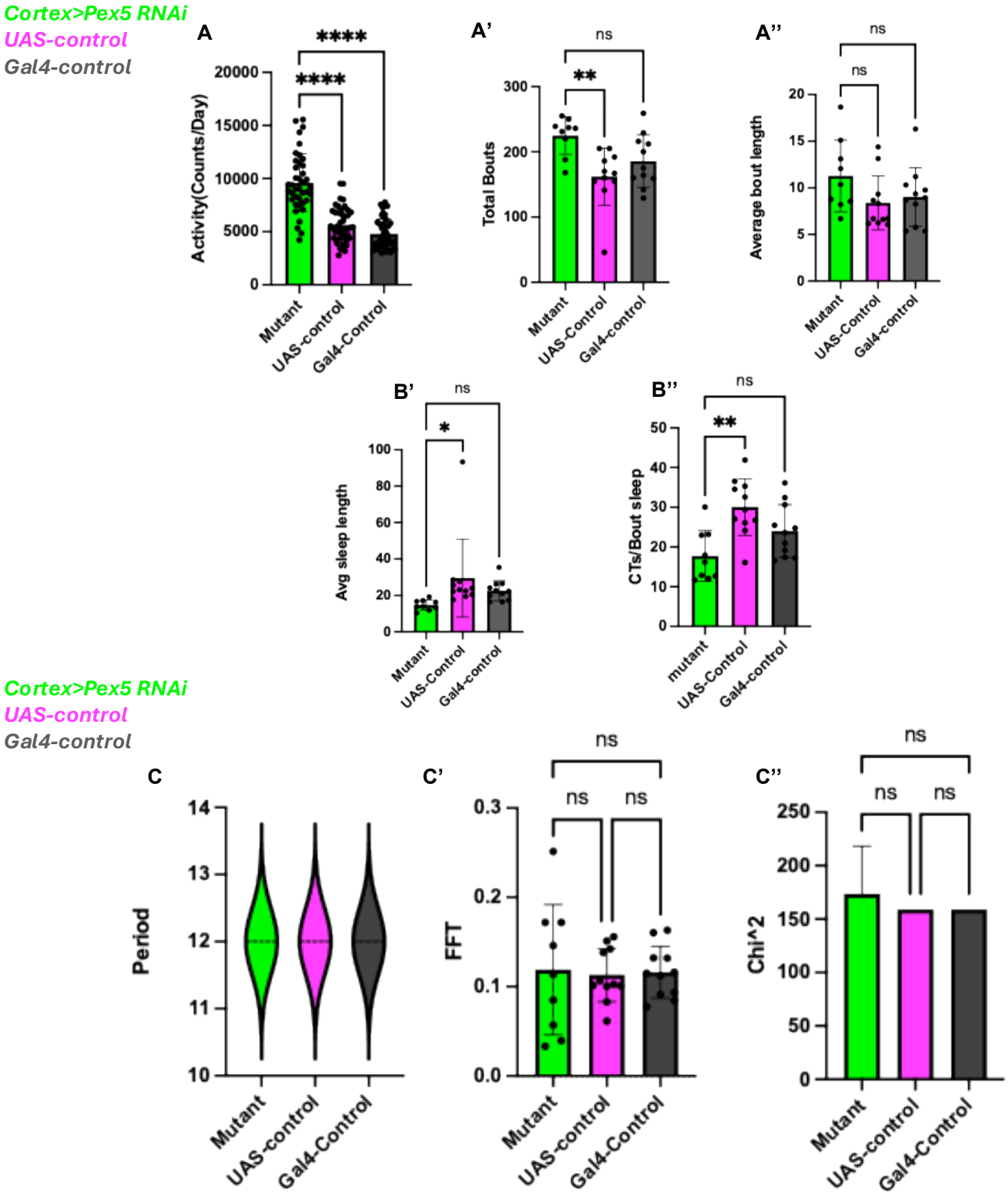

Figure 5- Supplemental

Figure S5, related to Figure 4– Sleep was measured for 12hr/12hr, light/dark cycle on an average for 4-5 days continuously for 5-day to 10-day old males; Individual black dots represent different biological replicates.

(A) Activity counts per day for *GMR77A03*-Gal4 crossed with *UAS-Pex5 RNAi* compared with parental genotypes – UAS-control and Gal4-control respectively.

(A') Total activity bouts per day for *GMR77A03*-Gal4 crossed with *UAS-Pex5 RNAi* compared with parental genotypes – UAS-control and Gal4-control respectively.

(A'') Average activity bout length for *GMR77A03*-Gal4 crossed with *UAS-Pex5 RNAi* compared with parental genotypes – UAS-control and Gal4-control respectively.

(A''') Sleep bouts for *GMR77A03*-Gal4 crossed with *UAS-Pex5 RNAi* compared with parental genotypes – UAS-control and Gal4-control respectively.

(B) Average Sleep length for *GMR77A03*-Gal4 crossed with *UAS-Pex5 RNAi* compared with parental genotypes – UAS-control and Gal4-control respectively.

(B') Counts total (CT) per bouts of sleep for *GMR77A03*-Gal4 crossed with *UAS-Pex5 RNAi* compared with parental genotypes – UAS-control and Gal4-control respectively.

(C) Period for *GMR77A03*-Gal4 crossed with *UAS-Pex5 RNAi* compared with parental genotypes – UAS-control and Gal4-control respectively.

(C') FFT/Fast Fourier Transform for *GMR77A03*-Gal4 crossed with *UAS-Pex5 RNAi* compared with parental genotypes – UAS-control and Gal4-control respectively.

(C'') Chi^2 for *GMR77A03*-Gal4 crossed with *UAS-Pex5 RNAi* compared with parental genotypes – UAS-control and Gal4-control respectively.

*ns-non-significant; $p < 0.05$, ** $p < 0.01$, *** $p < 0.001$, **** $p < 0.0001$ by Tukey's multiple comparisons test.

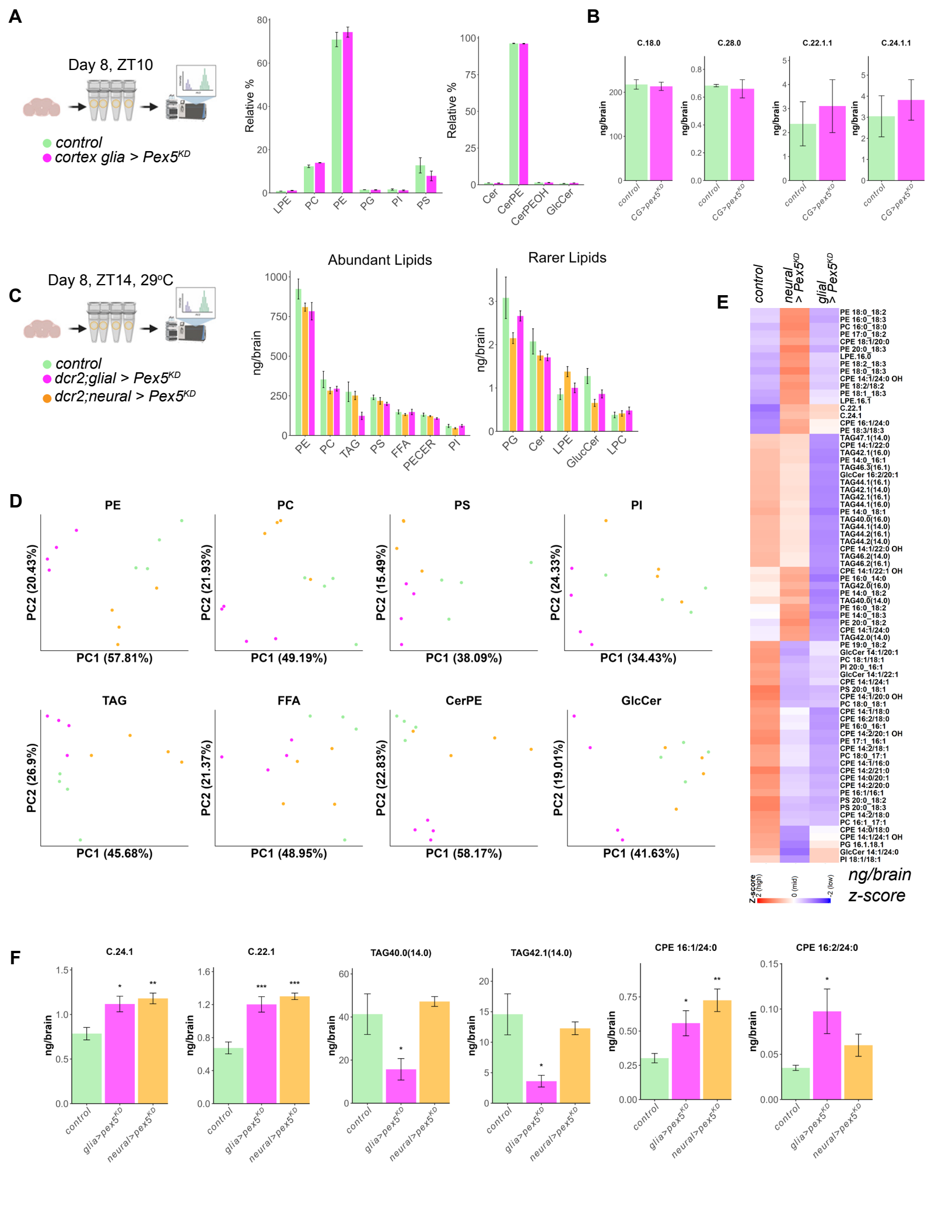
A
Day 8, ZT10
control
cortex glia > Pex5KD
Relative %
LPE
PC
PE
PG
PI
PS
Cer
CerPE
CerPEOH
GlcCer
B
C.18.0
C.28.0
C.22.1.1
C.24.1.1
ng/brain
control
CG>pex5KD
C
Day 8, ZT14, 29°C
control
dcr2;glial > Pex5KD
dcr2;neural > Pex5KD
Abundant Lipids
Rarer Lipids
ng/brain
PE
PC
TAG
PS
FFA
PECER
PI
PG
Cer
LPE
GlucCer
LPC
D
PE
PC
PS
PI
TAG
FFA
CerPE
GlcCer
PC2 (20.43%)
PC1 (57.81%)
PC2 (21.93%)
PC1 (49.19%)
PC2 (15.49%)
PC1 (38.09%)
PC2 (24.33%)
PC1 (34.43%)
PC2 (26.9%)
PC1 (45.68%)
PC2 (21.37%)
PC1 (48.95%)
PC2 (22.83%)
PC1 (58.17%)
PC2 (19.01%)
PC1 (41.63%)
E
control
neural > Pex5KD
glial > Pex5KD
PE 18:0_18:2
PE 16:0_18:3
PC 16:0_18:0
PE 17:0_18:2
CPE 18:1/20:0
PE 20:0_18:3
LPE.16.0
PE 18:2_18:3
PE 18:0_18:3
CPE 14:1/24:0 OH
PE 18:2/18:2
PE 18:1_18:3
LPE.16.1
C.22.1
C.24.1
CPE 16:1/24:0
PE 18:3/18:3
TAG47.1(14.0)
CPE 14:1/22:0
TAG42.1(16.0)
PE 14:0_16:1
TAG46.3(16.1)
GlcCer 16:2/20:1
TAG44.1(16.1)
TAG42.1(14.0)
TAG42.1(16.1)
TAG44.1(16.0)
PE 14:0_18:1
TAG40.0(16.0)
TAG44.1(14.0)
TAG44.2(16.1)
TAG44.2(14.0)
CPE 14:1/22:0 OH
TAG46.2(14.0)
TAG46.2(16.1)
CPE 14:1/22:1 OH
PE 16:0_14:0
TAG42.0(16.0)
PE 14:0_18:2
TAG40.0(14.0)
PE 16:0_18:2
PE 14:0_18:3
PE 20:0_18:2
CPE 14:1/24:0
TAG42.0(14.0)
PE 19:0_18:2
GlcCer 14:1/20:1
PC 18:1/18:1
PI 20:0_16:1
GlcCer 14:1/22:1
CPE 14:1/24:1
PS 20:0_18:1
CPE 14:1/20:0 OH
PC 18:0_18:1
CPE 14:1/18:0
CPE 16:2/18:0
PE 16:0_16:1
CPE 14:2/20:1 OH
PE 17:1_16:1
CPE 14:2/18:1
PC 18:0_17:1
CPE 14:1/16:0
CPE 14:2/21:0
CPE 14:0/20:1
CPE 14:2/20:0
PE 16:1/16:1
PS 20:0_18:2
PS 20:0_18:3
CPE 14:2/18:0
PC 16:1_17:1
CPE 14:0/18:0
CPE 14:1/24:1 OH
PG 16.1.18.1
GlcCer 14:1/24:0
PI 18:1/18:1
Z-score
2 (high)
0 (mid)
-2 (low)
ng/brain
z-score
F
C.24.1
C.22.1
TAG40.0(14.0)
TAG42.1(14.0)
CPE 16:1/24:0
CPE 16:2/24:0
ng/brain
control
glia>pex5KD
neural>pex5KD

Figure S6, related to Figure 5

(A) 3 tubes of 20 brains for control (green) and *cortex-glia>Pex5*^{KD} (magenta) were dissected at 8 days of age (female, 25°C, matching prior experiments).The relative % distribution of major lipids is unchanged.

(B) Free fatty acid species in controls (green) and *cortex-glia>Pex5*^{KD} (magenta).

(C) 4 tubes of 20 brains for control (*+/pex5*^{KD}*;* green), pan-glial (*dcr2;repo-GAL4> Pex5*^{KD};magenta) and pan-neuronal (*dcr2;nSyb-GAL4> Pex5*^{KD};orange) were dissected at 8 days of age (female, 29°C). Abundant and rarer lipids are quantified in ng/brain.

(D) Principal component analysis of major lipid families (PE = phosphatidylethanolamine; PC= phosphatidylcholine; PS = phosphatidylserine; PI = phosphatidylinositol; TAG = triacylglycerol; FFA = free fatty acid; CerPE = Ceramide Phosphoethanolamine, CPE; and GlcCer = Glucosylceramide). Control tubes = green, pan-glial (*dcr2;repo-GAL4> Pex5*^{KD}) = magenta, and pan-neuronal tubes (*dcr2;nSyb-GAL4> Pex5*^{KD}) = orange.

(E) Heatmap of z-scored ng/brain lipid abundance between pan-glial (*dcr2;repo-GAL4> Pex5*^{KD}), pan-neuronal (*dcr2;nSyb-GAL4> Pex5*^{KD}), and control *(+/pex5*^{KD}*)*

(F) Barplots of different lipids that are dysregulated by *Pex5* loss in glia (magenta) or neurons (orange) vs controls (green), in ng/brain.

*ns-non-significant; $p < 0.05$, ** $p < 0.01$, *** $p < 0.001$, **** $p < 0.0001$ by Tukey's multiple comparisons test.

RESOURCE AVAILABILITY

Lead contact

Correspondence should be directed to Anurag Das (anuragd7@iastate.edu)

Materials availability

All data and code reported in this paper will be shared by the lead contact (AD) upon request.

Acknowledgements

We thank Bai lab members for feedback during lab meetings. We thank Bloomington Drosophila Stock Center (NIH P40OD018537) for fly stocks. We thank FlyBase (NHGRI U41HG000739) for *Drosophila* gene annotation. We thank Kyu-Sun Lee for fly Pmp70 antibodies. We thank Abhilash Goswami for providing suggestions for the extraction of peroxisomal genes from publicly available single cell data. We thank Elizabeth McNeill, Amita Sehgal, Marc Tatar for sharing fly stocks. We thank Alicia Taylor from Elizabeth McNeill Lab for providing DAM5H-Trikinetics Drosophila Sleep Activity Monitoring system for our sleep studies. Graphical model figures were created with BioRender.com. This work was supported by NSF CAREER 2046984 and NIH R01AG058741 to HB. JPV is supported by the Sandler PBBR grant.

Author contributions

Conceptualization: AD, HB
Methodology: AD, IMRS, AK, JPV, HB
Investigation: AD, HK, LS, IMRS, JPV, HB
Visualization: AD, JPV, HB
Funding Acquisition: JPV, HB
Project Administration: AD, HB
Supervision: JPV, HB
Writing (original draft): AD
Writing (review & editing): AD, JPV

Declaration of interests

The authors declare no competing interests.

Key resources table

REAGENT or RESOURCE	SOURCE	IDENTIFIER
Antibodies		
Fly-PMP70	Huang et al., 2020	N/A
Anti-ELAV	DSHB	Rat-Elav-7E8A10 anti-elav
Anti-nc82	DSHB	nc82
Monoclonal Anti-FLAG	Sigma-Aldrich	F1804
Anti-SKL	Huang et al., 2020	N/A
Anti-GFP mAb	Cell Signaling Technology	2956
Experimental models: Organisms/strains		
D. melanogaster: *w*^{1118}	BDSC	Cat# 5905; RRID: BDSC_5905
D. melanogaster: *ywR*	A gift from Marc Tatar	N/A
D. melanogaster: *CantonS*	A gift from Elizabeth Mcneill	N/A
D. melanogaster: *per[01]*	BDSC	Cat# 80928; RRID: BDSC_80928
D. melanogaster: *w[1118]; P{y[+t7.7] w[+mC]=GMR77A03-GAL4}attP2*	BDSC	Cat# 39944; RRID: BDSC_39944
D. melanogaster: *w[1118]; P{y[+t7.7] w[+mC]=GMR54H02-GAL4}attP2*	BDSC	Cat# 45784; RRID: BDSC_45784
D. melanogaster: *y[1] v[1]; P{y[+t7.7] v[+t1.8]=TRiP.HMJ21920}attP40*	BDSC	Cat# 58064; RRID: BDSC_58064
D. melanogaster: *w[1118]; P{y[+t7.7] w[+mC]=GMR57C10-GAL4}attP2*	BDSC	Cat# 39171; RRID: BDSC_39171
D. melanogaster: *y[1] sc[*] v[1] sev[21]; P{y[+t7.7] v[+t1.8]=TRiP.HMS01530}attP40*	BDSC	Cat# 35780; RRID: BDSC_35780
D. melanogaster: *w[1118]; P{y[+t7.7] w[+mC]=GMR56F03-GAL4}attP2*	BDSC	Cat# 39157; RRID: BDSC_39157
D. melanogaster: *w[1118]; P{y[+t7.7] w[+mC]=GMR83E10-GAL4}attP2*	BDSC	Cat# 40362; RRID: BDSC_40362
D. melanogaster: *Pex5[FLAG-a1]/FM7a*	This paper	N/A
D. melanogaster: *w[1118]; P{w[+m*]=GAL4}repo/TM3, Sb[1]*	BDSC	Cat# 7415; RRID: BDSC_7415
D. melanogaster: *w[*]; P{w[+mC]=UAS-eYFP.PTS1}6*	BDSC	Cat# 64248; RRID: BDSC_64248
D. melanogaster: *y[1] w[*]; betaTub60D[Pin-Yt]/CyO; P{w[+mC]=UAS-mCD8::GFP.L}LL6*	BDSC	Cat# 5130; RRID: BDSC_5130
D. melanogaster: *w[*]; wg[Sp-1]/CyO; P{w[+m*]=alrm-GAL4.D}2*	BDSC	Cat# 67032; RRID: BDSC_67032
D. melanogaster: y[1] v[1]; P{y[+t7.7]=CaryP}Msp300[attP40]	BDSC	Cat# 36304; RRID: BDSC_36304
D. melanogaster: w[*]; P{w[+mC]=UAS-Clk.Delta}1	BDSC	Cat# 36318; RRID: BDSC_36318
Other		
BODIPY 493/503 Thermo Fisher Scientific	Thermo	Cat# D3922
Software and algorithms		
ImageJ	FIJI	imagej.net (USA)
Graphpad Prism 10	Graph Pad Software	Subscription ID :2814928
ADODE Illustrator 2020	ADOBE	N/A

Clock Lab Analysis 2	Actimetrrics	N/A
R Studio 2023.12.1 (4.3.1)	R	RRID: SCR_000432

EXPERIMENTAL MODEL AND METHOD DETAILS

Fly Husbandry and Stocks

Drosophila melanogaster were maintained at 25°C, 40% relative humidity and 12-hour light/dark cycle unless specified otherwise. Adults were reared on agar-based diet with 0.8% cornmeal, 10% sugar, and 2.5% yeast (unless otherwise noted). Fly stocks used in the present study are mentioned in the key resources table. Female flies were used in functional studies. For imaging experiments females adults aged 7-days were used unless otherwise specified. Flies and crosses were maintained in plastic vials and bottles with standard yeast-sucrose medium in a thermoregulated chamber at 25-degree Celsius following a 12:12 h light-dark cycle with 60% humidity. All experiments were performed 2-3 times independently.

***PEX5.FLAG* knock-in fly construct -** The *Pex5.FLAG* knock-in fly was generated using CRISPR/Cas9-mediated gene editing in *Drosophila*. The construct containing the *Pex5.FLAG* sequence was injected into *w1118* flies expressing *vas-Cas9* (BL51324). Injected G0 flies were crossed to an attached-X stock (HBF480/BL4559) to generate F1 progeny. F1 males carrying the *Pex5.FLAG* insertion were identified and crossed with various balancer stocks (FM7a, FM7c, or attached-X lines) to maintain and screen the modification. F2 progenies were selected based on genetic markers and crossed to establish stable lines. PCR and Western blot analyses using an anti-FLAG antibody confirmed successful FLAG tagging of Pex5.Homozygous *Pex5.FLAG* lines were generated and maintained. Additional heterozygous stocks were kept over FM7 balancer chromosomes. Western blot showed FLAG-tagged Pex5 bands (~70 kDa and 50 kDa). Sanger sequencing confirmed precise insertion of the FLAG tag. The final *Pex5.FLAG* lines were selected for future experiments.

Adult Brain Dissection - Adult *Drosophila* aged 7 days were anesthetized using ice. Using Dumont 3C tweezers, brain dissections were made immersed in Drosophila Schneider's Medium by first removing the proboscis and the head was separated to make the brain visible with intact optic lobes and by further removing the fat tissue. Brain tissues were immediately fixed within 60 seconds of dissection in 4% paraformaldehyde (PFA) and kept in rotator for 25 minutes at room temperature.

Immunohistochemistry - After brain tissues were fixed with 4% paraformaldehyde for 25 min at room temperature, this was followed by three rounds of washing for 10 minutes each in 0.2% PBST {5mL of 10x PBS + 45mL of dd H20 + add 0.1 mL (100uL) of triton} and subsequently kept in blocking solution of 5% NDS (normal donkey serum) for 1 hour. Tissues were then incubated with primary antibodies for 48 hours overnight at 4^0C, with secondary antibodies for another 48 hours at 4^0C. Samples were washed three times for 15minutes each in 0.2% PBST and then mounted with microfrost slides in Prolong Diamond(Life technologies) by carefully placing brain samples on 1% PBS on a glass

cover slip. Primary antibodies used were as follows: anti-Fly PMP70 (a gift from Kyu-Sun Lee Lab); anti-ELAV (0.1ml concentrate from DSHB); anti-FLAG(Thermo); anti-SKL; anti-nc82(DSHB). Dilution of 1:200 was used for secondary antibodies unless otherwise noted. Secondary antibodies included: 488 donkey anti-mouse, 647 donkey anti-mouse, , 488 anti-guinea Pig (Jackson ImmunoResearch Laboratories Inc, West Grove PA).

Confocal Microscopy - Images were captured using Olympus FV3000 laser scanning confocal (Olympus, Waltham, MA, USA). Using 60x oil-immersive lens and further with 5x digital zoom images of brain and zoomed in-images focused on cortex glial region surrounding neuronal cell body/soma were captured. All image analysis was performed on ImageJ/Fiji. Laser channels 488nm, 594nm and 647nm were respectively utilized.

Image Acquisition – All confocal acquired images were first converted to RGB images on FIJI and saved as TIF files for individual channels after creating composite images. These TIF generated files were copy/pasted on ADODE ILLUSTRATOR to create equal girds and boxes for image presentation.

Pearson Correlation Coefficient Analysis – *JACoP* plugin tool was installed in *FIJI* and utilized to automatically calculate the Pearson correlation coefficient (scale - 1 to 0; 1 being highest level of colocalization) between two 16-bit images in different color gradient (for example – between green and red laser channel acquired images). Please refer - *Bolte, S., & Cordelières, F. P. (2006). A guided tour into subcellular colocalization analysis in light microscopy. Journal of microscopy, 224(Pt 3), 213–232. https://doi.org/10.1111/j.1365-2818.2006.01706.x*

PTS1/SKL and PMP70 puncta counting – Stacked images were converted to individual channel images using FIJI ImageJ and using the *"Edit", "Selection", "Specify",* "*Width* was specified as 200" and "*Height* was specified as 200 " and multiple ROIs (atleast 3 to 5) for each replicate (n, number of replicates used were always 3 or more per condition) was analyzed using the "*Cell Counter*" function from "*Plugins*", "*Analyze*", "*Cell Counter*".

***PEX5.FLAG :* anti-flag mean intensity quantification to measure Pex5 oscillation** – Convert stacks to images; convert the images to 8-bit image; select image, go to adjust, go to threshold; select image, go to analyze, set measurement in value; select rectangle tool and select the required area; go to analyze and select measure.

Neutral lipid BODIPY 493/503 staining protocol – This method was developed for fixed tissue staining as follows: it performed after primary antibody & secondary antibody staining.10mM main stock of BODIPY 493/503 prepared from 10mg unit of BODIPY 493/503 by adding 5.2mL of DMSO and mixing it well till completely dissolved (1-2 hr at room temperature in mixer/shaker). It can be stored in minus 20-degree freezer. For working stocking - I have made 2mM in DMSO (800uL of DMSO + 200uL from prepared main stock of 10mM of BODPIY 493/503. It needs to be further diluted 1:100. Adult *Drosophila* brains to be stained in prepared BODIPY 493/503 for 10mins at room temperature (keep in covered with aluminum foil). To be followed by mounting of the sample tissue & imaging (confocal). Use 50% glycerol for mounting tissue.

Lipid droplet quantification - the uploaded color images were converted into an 8-bit grayscale image by selecting the "*Image*", *Type*", and "*8-bit*". A threshold defined by the range of minimum and maximum values of the RGB color (16 and 255 arbitrary units) was selected to convert the grayscale image to a binary image by selecting the options "*Image*", "*Adjust*", and *Threshold*". After all parameters from the "*Threshold*" option were setup, "*Set*" was selected. The "*Analyze Particles*" macro was run by first selecting the "*Analyze*" option and then the macro "*Analyze Particles*". Hereafter, maximum and minimum values for the size and circularity of the objects was selected. Once all parameters from the "*Analyze Particles*" macro were setup, "*OK*" was selected to run the automated analysis. A separate "*Results*" window provided the area of each particle identified and a separate "*Summary*" window provided the output variables: total number of identified particles, the total positive lipid area (in pixels), the average size of each particle (in pixels).

Lipidomics. Workflow was adapted from *Vaughen et al., 2022*[96]. 20 Brains (female, 8 days) were dissected rapidly on ice-cold 1xPBS and snap frozen in 90% methanol (v/v). A modified folch extraction was used and separate columns and standards were run on an agilent triplequad. Data were analyzed in R studio, with FDR corrected t-test. Five brains were analyzed for triglycerides and free fatty acids. Brain total lipids containing internal standards (ISTD) were extracted as described Vaughen et al, 2022. ISTD used included Equisplash™ LIPIDOMIX® Quantitative Mass Spec Internal Standard (Avanti #330731) and Oleic Acid-d9 (Avanti #861809).

For free fatty acid analysis, an Agilent Zorbax RX-Sil column 3.0 x 100 mm, 1.8 µm particle size was used. The total LC run time was 19 min (with 2.5 min post-run) at a flow rate of 0.3 µL/min. Mobile phase A was composed of isopropanol/hexane/water (58:40:2, v/v) with 5mM ammonium acetate and 0.1% acetic acid. Mobile phase B consisted of isopropanol/hexane/water (50:40:10, v/v) with 5mM ammonium acetate and 0.1% acetic acid. Gradient elution consisted of 0 to 17 min of 0% mobile phase B and an increase from 17 to 18 min until 100% of mobile phase B and after 18 min the mobile phase decreased to 0% for 1 more min. The Agilent 6430 Triple-Quad LC/MS system (Santa Clara, CA) was operated in negative mode. Free fatty acids were identified as $[M - H]^-$ and it was run as a pseudoMRM.

Triglycerides were separated as described by Kehelpannala et al., 2020[97]. An InfinityLab Poroshell 120 EC-C18 2.1 × 100 mm (2.7-Micron particle size) column (Agilent, USA) operated at 55 °C using an Agilent 1260 Infinity LC system (Santa Clara, CA). The solvent system consisted of Mobile phase A acetonitrile (ACN)-water (60:40, v/v) and mobile phase B and isopropanol (IPP)-ACN (90/10, v/v) both containing 10 mM ammonium formate. The gradient was starting with a flow rate of 0.26 mL/min and it was set to first a 0–1.5 min isocratic elution with 32% B which was then increased to 45% B from 1.5 to 4 min, then to 52% B from 4 to 5 min followed by an increase to 58% B from 5 to 8 min. Next, the gradient was increased to 66% B from 8 to 11 min followed by an increase to 70% B from 11 to 14 min and an increase to 75% B from 14 to 18 min. Then, from 18 to 21 min B was increased to 97% and B was maintained at 97% from 21 to 25 min. Finally, solvent B was decreased to 32% from 25 to 25.10 min, and B was maintained at 32% for another 4.9 min for column reequilibration. The Agilent 6430 Triple-Quad LC/MS system (Santa Clara, CA) was operated in positive mode. Triglycerides were

identified as $[M + NH4]^+$ molecular ions representing the neutral loss of the fatty acid. The collision voltage was 21 eV.

Gas-phase ions of various lipid species were obtained using electrospray ionization (ESI), with the electrospray needle held at -3,500 V (+) and 3,000 V (–). Data acquisition and analysis was carried out using Agilent Mass Hunter software.

Sleep Behavioral Assay - For sleep behavioral analysis in light-dark conditions (12hr light/12-hr dark) young mutant *Pex5* flies crosses with respective glial or neural specific driver with comparable young parental control *(UAS-control – w^{1118} & GAL4-control – attP40)* have been utilized. We used the *Drosophila* Activity Monitors (DAMs, Trikinetics). 5-10 day old (typically males as egg laying activity of mated females will disrupt circadian reading output) was used and loaded into tubes, and sleep data was recorded until day 10 for a minimum of 3 continuous days after 1st day or 24 hours of entrainment (data from entrainment was not used for analysis). We utilized data from day 6 to day 10 after developmental sleep has been completed. Cessation of activity for 5 mins was used as a proxy for sleep; flies that were inactive for 12h prior to endpoint of the analyzed period will be inferred to be dead and omitted from analysis. Data was analyzed in ClockLab software and Shiny R-DAM separately. (https://karolcichewicz.shinyapps.io/shinyr-dam/).

For free-running rhythmicity assay to assess circadian rhythms of *cortex>UAS-Pex5 RNAi* and its respective parental controls *(UAS-control – w^{1118} & GAL4-control – attP40);* after 4 complete days in light/dark cycle the flies were covered with silver aluminum foil & opaque black cardboard for dark/dark (D/D) conditions after evening 6P.M. (subjective night-time of flies). Entrainment in (D/D) conditions was done for 24 hours and flies were kept in dark-dark conditions for a total of six complete and consecutive days in (D/D) conditions to determine if Pex5 RNAi knockdown disrupted circadian rhythms in cortex glia specifically. Data was analyzed in Clock lab software. Please refer supplemental excel sheets (supplemental 5A).

Heat Map Hierarchical Clustering & Generation – Code was generated by Anurag Das on PositCloud which replicates JUPYTER notebook environment. Code can be shared with request to author. After hierarchical clustering, data was further aggregated and cleaned up manually on GraphPad Prism to add colors of choice in representative value scale.

QUANTIFICATION AND STATISTICAL ANALYSIS - GraphPad Prism (GraphPad Software Version 10) was used for statistical analysis. Unpaired two-tailed Student's t-test for comparison between 2 groups or one-way ANOVA (Sidak's and Tukey multiple comparison) was performed to compare the mean value between control and treatment groups of more than two groups respectively. Lipidomics data were analyzed and plotted in R studio.

References

1. Wanders RJA, Baes M, Ribeiro D, Ferdinandusse S, Waterham HR. The physiological functions of human peroxisomes. *Physiological Reviews*. 2023;103(1):957-1024. doi:10.1152/physrev.00051.2021

2. Ding L, Sun W, Balaz M, et al. Peroxisomal β-oxidation acts as a sensor for intracellular fatty acids and regulates lipolysis. *Nat Metab*. 2021;3(12):1648-1661. doi:10.1038/s42255-021-00489-2

3. Lodhi IJ, Semenkovich CF. Peroxisomes: a nexus for lipid metabolism and cellular signaling. *Cell Metab*. 2014;19(3):380-392. doi:10.1016/j.cmet.2014.01.002

4. Sodders M, Das A, Bai H. Glial peroxisome dysfunction induces axonal swelling and neuroinflammation in Drosophila. *G3 Genes|Genomes|Genetics*. 2025;15(1):jkae243. doi:10.1093/g3journal/jkae243

5. Kassmann CM, Lappe-Siefke C, Baes M, et al. Axonal loss and neuroinflammation caused by peroxisome-deficient oligodendrocytes. *Nat Genet*. 2007;39(8):969-976. doi:10.1038/ng2070

6. Kleinecke S, Richert S, de Hoz L, et al. Peroxisomal dysfunctions cause lysosomal storage and axonal Kv1 channel redistribution in peripheral neuropathy. Ackerman SL, ed. *eLife*. 2017;6:e23332. doi:10.7554/eLife.23332

7. Santos MJ, Henderson SC, Moser AB, Moser HW, Lazarow PB. Peroxisomal ghosts are intracellular structures distinct from lysosomal compartments in Zellweger syndrome: a confocal laser scanning microscopy study. *Biol Cell*. 2000;92(2):85-94. doi:10.1016/s0248-4900(00)89016-4

8. Soliman K, Göttfert F, Rosewich H, Thoms S, Gärtner J. Super-resolution imaging reveals the sub-diffraction phenotype of Zellweger Syndrome ghosts and wild-type peroxisomes. *Sci Rep*. 2018;8(1):7809. doi:10.1038/s41598-018-24119-2

9. Krause C, Rosewich H, Woehler A, Gärtner J. Functional analysis of PEX13 mutation in a Zellweger syndrome spectrum patient reveals novel homooligomerization of PEX13 and its role in human peroxisome biogenesis. *Human Molecular Genetics*. 2013;22(19):3844-3857. doi:10.1093/hmg/ddt238

10. De Munter S, Verheijden S, Régal L, Baes M. Peroxisomal Disorders: A Review on Cerebellar Pathologies. *Brain Pathol*. 2015;25(6):663-678. doi:10.1111/bpa.12290

11. Berger J, Dorninger F, Forss-Petter S, Kunze M. Peroxisomes in brain development and function. *Biochim Biophys Acta*. 2016;1863(5):934-955. doi:10.1016/j.bbamcr.2015.12.005

12. Abe Y, Honsho M, Itoh R, et al. Peroxisome biogenesis deficiency attenuates the BDNF-TrkB pathway-mediated development of the cerebellum. *Life Sci Alliance*. 2018;1(6):e201800062. doi:10.26508/lsa.201800062

13. Smith MD, Schnell DJ. Peroxisomal protein import. the paradigm shifts. *Cell*. 2001;105(3):293-296. doi:10.1016/s0092-8674(01)00337-3

14. Dammai V, Subramani S. The human peroxisomal targeting signal receptor, Pex5p, is translocated into the peroxisomal matrix and recycled to the cytosol. *Cell*. 2001;105(2):187-196. doi:10.1016/s0092-8674(01)00310-5

15. Smith JJ, Aitchison JD. Peroxisomes take shape. *Nat Rev Mol Cell Biol*. 2013;14(12):803-817. doi:10.1038/nrm3700

16. Huang K, Miao T, Chang K, et al. Impaired peroxisomal import in Drosophila oenocytes causes cardiac dysfunction by inducing upd3 as a peroxikine. *Nat Commun*. 2020;11(1):2943. doi:10.1038/s41467-020-16781-w

17. Bottelbergs A, Verheijden S, Hulshagen L, et al. Axonal integrity in the absence of functional peroxisomes from projection neurons and astrocytes. *Glia*. 2010;58(13):1532-1543. doi:10.1002/glia.21027

18. Di Cara F, Rachubinski RA, Simmonds AJ. Distinct Roles for Peroxisomal Targeting Signal Receptors Pex5 and Pex7 in Drosophila. *Genetics*. 2019;211(1):141-149. doi:10.1534/genetics.118.301628

19. Kremer MC, Jung C, Batelli S, Rubin GM, Gaul U. The glia of the adult Drosophila nervous system. *Glia*. 2017;65(4):606-638. doi:10.1002/glia.23115

20. Awasaki T, Lai SL, Ito K, Lee T. Organization and postembryonic development of glial cells in the adult central brain of Drosophila. *J Neurosci*. 2008;28(51):13742-13753. doi:10.1523/JNEUROSCI.4844-08.2008

21. Freeman MR. Drosophila Central Nervous System Glia. *Cold Spring Harb Perspect Biol*. 2015;7(11):a020552. doi:10.1101/cshperspect.a020552

22. Coutinho-Budd J, Freeman MR, Ackerman S. Glial Regulation of Circuit Wiring, Firing, and Expiring in the Drosophila Central Nervous System. *Cold Spring Harb Perspect Biol*. 2024;16(12):a041347. doi:10.1101/cshperspect.a041347

23. Yildirim K, Petri J, Kottmeier R, Klämbt C. Drosophila glia: Few cell types and many conserved functions. *Glia*. 2019;67(1):5-26. doi:10.1002/glia.23459

24. Dubowy C, Sehgal A. Circadian Rhythms and Sleep in Drosophila melanogaster. *Genetics*. 2017;205(4):1373-1397. doi:10.1534/genetics.115.185157

25. Glou EL, Seugnet L, Shaw PJ, Preat T, Goguel V. Circadian Modulation of Consolidated Memory Retrieval Following Sleep Deprivation in Drosophila. *Sleep*. 2012;35(10):1377-1384. doi:10.5665/sleep.2118

26. Chouhan NS, Wolf R, Helfrich-Förster C, Heisenberg M. Flies Remember the Time of Day. *Current Biology*. 2015;25(12):1619-1624. doi:10.1016/j.cub.2015.04.032

27. Hendricks JC, Sehgal A. Why a Fly? Using Drosophila to Understand the Genetics of Circadian Rhythms and Sleep. *Sleep*. 2004;27(2):334-342. doi:10.1093/sleep/27.2.334

28. Allada R, Chung BY. Circadian organization of behavior and physiology in Drosophila. *Annu Rev Physiol*. 2010;72:605-624. doi:10.1146/annurev-physiol-021909-135815

29. Cavey M, Collins B, Bertet C, Blau J. Circadian rhythms in neuronal activity propagate through output circuits. *Nat Neurosci*. 2016;19(4):587-595. doi:10.1038/nn.4263

30. Ezagouri S, Asher G. Circadian control of mitochondrial dynamics and functions. *Current Opinion in Physiology*. 2018;5:25-29. doi:10.1016/j.cophys.2018.05.008

31. Ng FS, Tangredi MM, Jackson FR. Glial cells physiologically modulate clock neurons and circadian behavior in a calcium-dependent manner. *Curr Biol*. 2011;21(8):625-634. doi:10.1016/j.cub.2011.03.027

32. Rieger D, Shafer OT, Tomioka K, Helfrich-Förster C. Functional Analysis of Circadian Pacemaker Neurons in Drosophila melanogaster. *J Neurosci*. 2006;26(9):2531-2543. doi:10.1523/JNEUROSCI.1234-05.2006

33. Dopp J, Ortega A, Davie K, Poovathingal S, Baz ES, Liu S. Single-cell transcriptomics reveals that glial cells integrate homeostatic and circadian processes to drive sleep–wake cycles. *Nat Neurosci*. 2024;27(2):359-372. doi:10.1038/s41593-023-01549-4

34. Damulewicz M, Doktór B, Baster Z, Pyza E. The Role of Glia Clocks in the Regulation of Sleep in Drosophila melanogaster. *J Neurosci*. 2022;42(36):6848-6860. doi:10.1523/JNEUROSCI.2340-21.2022

35. Helfrich-Förster C. The period clock gene is expressed in central nervous system neurons which also produce a neuropeptide that reveals the projections of circadian pacemaker cells within the brain of Drosophila melanogaster. *Proc Natl Acad Sci USA*. 1995;92(2):612-616. doi:10.1073/pnas.92.2.612

36. Mazzoni EO, Desplan C, Blau J. Circadian pacemaker neurons transmit and modulate visual information to control a rapid behavioral response. *Neuron*. 2005;45(2):293-300. doi:10.1016/j.neuron.2004.12.038

37. Taghert PH. Circadian Pacemakers: How Clock Properties Relate To Their Cellular Properties. *Current Biology*. 2011;21(21):R894-R896. doi:10.1016/j.cub.2011.09.041

38. Neufeld-Cohen A, Robles MS, Aviram R, et al. Circadian control of oscillations in mitochondrial rate-limiting enzymes and nutrient utilization by PERIOD proteins. *Proc Natl Acad Sci U S A*. 2016;113(12):E1673-1682. doi:10.1073/pnas.1519650113

39. Ezagouri S, Zwighaft Z, Sobel J, et al. Physiological and Molecular Dissection of Daily Variance in Exercise Capacity. *Cell Metab*. 2019;30(1):78-91.e4. doi:10.1016/j.cmet.2019.03.012

40. Zhang R, Lahens NF, Ballance HI, Hughes ME, Hogenesch JB. A circadian gene expression atlas in mammals: implications for biology and medicine. *Proc Natl Acad Sci U S A*. 2014;111(45):16219-16224. doi:10.1073/pnas.1408886111

41. Gould SJ, Collins CS. Peroxisomal-protein import: is it really that complex? *Nat Rev Mol Cell Biol*. 2002;3(5):382-389. doi:10.1038/nrm807

42. Skowyra ML, Feng P, Rapoport TA. Towards solving the mystery of peroxisomal matrix protein import. *Trends in Cell Biology*. 2024;34(5):388-405. doi:10.1016/j.tcb.2023.08.005

43. Korotkova D, Borisyuk A, Guihur A, et al. Fluorescent fatty acid conjugates for live cell imaging of peroxisomes. *Nat Commun*. 2024;15(1):4314. doi:10.1038/s41467-024-48679-2

44. Chung HL, Wangler MF, Marcogliese PC, et al. Loss- or Gain-of-Function Mutations in ACOX1 Cause Axonal Loss via Different Mechanisms. *Neuron*. 2020;106(4):589-606.e6. doi:10.1016/j.neuron.2020.02.021

45. Yin J, Shao Y, Huang F, et al. Peroxisomal membrane protein PMP70 confers drug resistance in colorectal cancer. *Cell Death Dis*. 2025;16(1):293. doi:10.1038/s41419-025-07572-6

46. Faust JE, Manisundaram A, Ivanova PT, et al. Peroxisomes are required for lipid metabolism and muscle function in Drosophila melanogaster. *PLoS One*. 2014;9(6):e100213. doi:10.1371/journal.pone.0100213

47. Kunduri G, Turner-Evans D, Konya Y, et al. Defective cortex glia plasma membrane structure underlies light-induced epilepsy in cpes mutants. *Proc Natl Acad Sci U S A*. 2018;115(38):E8919-E8928. doi:10.1073/pnas.1808463115

48. Melom JE, Littleton JT. Mutation of a NCKX eliminates glial microdomain calcium oscillations and enhances seizure susceptibility. *J Neurosci*. 2013;33(3):1169-1178. doi:10.1523/JNEUROSCI.3920-12.2013

49. Weiss S, Melom JE, Ormerod KG, Zhang YV, Littleton JT. Glial Ca2+signaling links endocytosis to K+ buffering around neuronal somas to regulate excitability. Westbrook GL, Davis GW, Davis GW, Zinn K, eds. *eLife*. 2019;8:e44186. doi:10.7554/eLife.44186

50. Spéder P, Brand AH. Systemic and local cues drive neural stem cell niche remodelling during neurogenesis in Drosophila. Banerjee U, ed. *eLife*. 2018;7:e30413. doi:10.7554/eLife.30413

51. Bailey AP, Koster G, Guillermier C, et al. Antioxidant Role for Lipid Droplets in a Stem Cell Niche of *Drosophila*. *Cell*. 2015;163(2):340-353. doi:10.1016/j.cell.2015.09.020

52. Prolo LM, Takahashi JS, Herzog ED. Circadian Rhythm Generation and Entrainment in Astrocytes. *J Neurosci*. 2005;25(2):404-408. doi:10.1523/JNEUROSCI.4133-04.2005

53. Ewer J, Frisch B, Hamblen-Coyle MJ, Rosbash M, Hall JC. Expression of the period clock gene within different cell types in the brain of Drosophila adults and mosaic analysis of these cells' influence on circadian behavioral rhythms. *J Neurosci*. 1992;12(9):3321-3349. doi:10.1523/JNEUROSCI.12-09-03321.1992

54. Brancaccio M, Edwards MD, Patton AP, et al. Cell-autonomous clock of astrocytes drives circadian behavior in mammals. *Science*. 2019;363(6423):187-192. doi:10.1126/science.aat4104

55. Lananna BV, Nadarajah CJ, Izumo M, et al. Cell-Autonomous Regulation of Astrocyte Activation by the Circadian Clock Protein BMAL1. *Cell Rep*. 2018;25(1):1-9.e5. doi:10.1016/j.celrep.2018.09.015

56. Damulewicz M, Doktór B, Baster Z, Pyza E. The Role of Glia Clocks in the Regulation of Sleep in Drosophila melanogaster. *J Neurosci*. 2022;42(36):6848-6860. doi:10.1523/JNEUROSCI.2340-21.2022

57. Tanoue S, Krishnan P, Krishnan B, Dryer SE, Hardin PE. Circadian Clocks in Antennal Neurons Are Necessary and Sufficient for Olfaction Rhythms in Drosophila. *Current Biology*. 2004;14(8):638-649. doi:10.1016/j.cub.2004.04.009

58. Li Y, Haynes P, Zhang SL, Yue Z, Sehgal A. Ecdysone acts through cortex glia to regulate sleep in Drosophila. Ramaswami M, VijayRaghavan K, Keene AC, eds. *eLife*. 2023;12:e81723. doi:10.7554/eLife.81723

59. Haynes PR, Pyfrom ES, Li Y, et al. A neuron–glia lipid metabolic cycle couples daily sleep to mitochondrial homeostasis. *Nat Neurosci*. 2024;27(4):666-678. doi:10.1038/s41593-023-01568-1

60. Kong J, Ji Y, Jeon YG, et al. Spatiotemporal contact between peroxisomes and lipid droplets regulates fasting-induced lipolysis via PEX5. *Nat Commun*. 2020;11(1):578. doi:10.1038/s41467-019-14176-0

61. Wright ZJ, Tharp NE, Bartel B. ER nests are specialized ER subdomains in Arabidopsis where peroxisomes and lipid droplets form. *Developmental Cell*. 2025;0(0). doi:10.1016/j.devcel.2025.03.005

62. Li N, Hua B, Chen Q, et al. A sphingolipid-mTORC1 nutrient-sensing pathway regulates animal development by an intestinal peroxisome relocation-based gut-brain crosstalk. *Cell Rep*. 2022;40(4):111140. doi:10.1016/j.celrep.2022.111140

63. Drosophila models uncover substrate channeling effects on phospholipids and sphingolipids in peroxisomal biogenesis disorders | PLOS One. Accessed June 17, 2025. https://journals.plos.org/plosone/article?id=10.1371/journal.pone.0324143

64. Huang F, Cai F, Dahabieh MS, et al. Peroxisome disruption alters lipid metabolism and potentiates antitumor response with MAPK-targeted therapy in melanoma. *J Clin Invest*. 2023;133(20):e166644. doi:10.1172/JCI166644

65. Theisen EK, Rivas-Serna IM, Lee RJ, et al. Glia phagocytose neuronal sphingolipids to infiltrate developing synapses. *bioRxiv*. Published online April 22, 2025:2025.04.14.648777. doi:10.1101/2025.04.14.648777

66. Halassa MM, Fellin T, Takano H, Dong JH, Haydon PG. Synaptic islands defined by the territory of a single astrocyte. *J Neurosci*. 2007;27(24):6473-6477. doi:10.1523/JNEUROSCI.1419-07.2007

67. Allen NJ, Barres BA. Glia — more than just brain glue. *Nature*. 2009;457(7230):675-677. doi:10.1038/457675a

68. Hanani M. Satellite glial cells in sensory ganglia: from form to function. *Brain Research Reviews*. 2005;48(3):457-476. doi:10.1016/j.brainresrev.2004.09.001

69. Takasaki C, Yamasaki M, Uchigashima M, Konno K, Yanagawa Y, Watanabe M. Cytochemical and cytological properties of perineuronal oligodendrocytes in the mouse cortex. *Eur J Neurosci*. 2010;32(8):1326-1336. doi:10.1111/j.1460-9568.2010.07377.x

70. Kis V, Barti B, Lippai M, Sass M. Specialized Cortex Glial Cells Accumulate Lipid Droplets in Drosophila melanogaster. *PLOS ONE*. 2015;10(7):e0131250. doi:10.1371/journal.pone.0131250

71. Silva B, Mantha OL, Schor J, et al. Glia fuel neurons with locally synthesized ketone bodies to sustain memory under starvation. *Nat Metab*. 2022;4(2):213-224. doi:10.1038/s42255-022-00528-6

72. Buchanan RL, Benzer S. Defective Glia in the Drosophila Brain Degeneration Mutant drop-dead. *Neuron*. 1993;10(5):839-850. doi:10.1016/0896-6273(93)90200-B

73. Dumstrei K, Wang F, Hartenstein V. Role of DE-cadherin in neuroblast proliferation, neural morphogenesis, and axon tract formation in Drosophila larval brain development. *J Neurosci*. 2003;23(8):3325-3335. doi:10.1523/JNEUROSCI.23-08-03325.2003

74. Schmitt K, Grimm A, Dallmann R, et al. Circadian Control of DRP1 Activity Regulates Mitochondrial Dynamics and Bioenergetics. *Cell Metab*. 2018;27(3):657-666.e5. doi:10.1016/j.cmet.2018.01.011

75. Maury E, Ramsey KM, Bass J. Circadian rhythms and metabolic syndrome: from experimental genetics to human disease. *Circ Res*. 2010;106(3):447-462. doi:10.1161/CIRCRESAHA.109.208355

76. Chua ECP, Shui G, Lee ITG, et al. Extensive diversity in circadian regulation of plasma lipids and evidence for different circadian metabolic phenotypes in humans. *Proc Natl Acad Sci U S A*. 2013;110(35):14468-14473. doi:10.1073/pnas.1222647110

77. Amatobi KM, Ozbek-Unal AG, Schäbler S, et al. The circadian clock is required for rhythmic lipid transport in Drosophila in interaction with diet and photic condition. *J Lipid Res*. 2023;64(10):100417. doi:10.1016/j.jlr.2023.100417

78. Akhtar RA, Reddy AB, Maywood ES, et al. Circadian cycling of the mouse liver transcriptome, as revealed by cDNA microarray, is driven by the suprachiasmatic nucleus. *Curr Biol*. 2002;12(7):540-550. doi:10.1016/s0960-9822(02)00759-5

79. Kita Y, Shiozawa M, Jin W, et al. Implications of circadian gene expression in kidney, liver and the effects of fasting on pharmacogenomic studies. *Pharmacogenetics*. 2002;12(1):55-65. doi:10.1097/00008571-200201000-00008

80. McCarthy JJ, Andrews JL, McDearmon EL, et al. Identification of the circadian transcriptome in adult mouse skeletal muscle. *Physiol Genomics*. 2007;31(1):86-95. doi:10.1152/physiolgenomics.00066.2007

81. Panda S, Antoch MP, Miller BH, et al. Coordinated transcription of key pathways in the mouse by the circadian clock. *Cell*. 2002;109(3):307-320. doi:10.1016/s0092-8674(02)00722-5

82. Reddy AB, Karp NA, Maywood ES, et al. Circadian orchestration of the hepatic proteome. *Curr Biol*. 2006;16(11):1107-1115. doi:10.1016/j.cub.2006.04.026

83. Zvonic S, Ptitsyn AA, Conrad SA, et al. Characterization of peripheral circadian clocks in adipose tissues. *Diabetes*. 2006;55(4):962-970. doi:10.2337/diabetes.55.04.06.db05-0873

84. Storch KF, Lipan O, Leykin I, et al. Extensive and divergent circadian gene expression in liver and heart. *Nature*. 2002;417(6884):78-83. doi:10.1038/nature744

85. Delventhal R, Barber AF. Sensory integration: Time and temperature regulate fly siesta. *Curr Biol*. 2022;32(19):R1020-R1022. doi:10.1016/j.cub.2022.08.072

86. Crane DI, Maxwell MA, Paton BC. PEX1 mutations in the Zellweger spectrum of the peroxisome biogenesis disorders. *Hum Mutat*. 2005;26(3):167-175. doi:10.1002/humu.20211

87. Krause C, Rosewich H, Woehler A, Gärtner J. Functional analysis of PEX13 mutation in a Zellweger syndrome spectrum patient reveals novel homooligomerization of PEX13 and its role in human peroxisome biogenesis. *Human Molecular Genetics*. 2013;22(19):3844-3857. doi:10.1093/hmg/ddt238

88. Mast FD, Li J, Virk MK, Hughes SC, Simmonds AJ, Rachubinski RA. A Drosophila model for the Zellweger spectrum of peroxisome biogenesis disorders. *Dis Model Mech*. 2011;4(5):659-672. doi:10.1242/dmm.007419

89. Shafer OT, Keene AC. The Regulation of Drosophila Sleep. *Curr Biol*. 2021;31(1):R38-R49. doi:10.1016/j.cub.2020.10.082

90. Jagannathan SR, Jeans T, Van De Poll MN, van Swinderen B. Multivariate classification of multichannel long-term electrophysiology data identifies different sleep stages in fruit flies. *Science Advances*. 2024;10(8):eadj4399. doi:10.1126/sciadv.adj4399

91. Abhilash L, Shafer OT. A two-process model of Drosophila sleep reveals an inter-dependence between circadian clock speed and the rate of sleep pressure decay. *Sleep*. 2024;47(2):zsad277. doi:10.1093/sleep/zsad277

92. Borbély A. The two-process model of sleep regulation: Beginnings and outlook. *Journal of Sleep Research*. 2022;31(4):e13598. doi:10.1111/jsr.13598

93. Solis BL, Koch R, Nagoshi E. Circadian clock-independent ultradian rhythms in lipid metabolism in the Drosophila fat body. *Journal of Biological Chemistry*. 2025;301(6). doi:10.1016/j.jbc.2025.110245

94. Molusky MM, Ma D, Buelow K, Yin L, Lin JD. Peroxisomal localization and circadian regulation of ubiquitin-specific protease 2. *PLoS One*. 2012;7(11):e47970. doi:10.1371/journal.pone.0047970

95. Sang D, Lin K, Yang Y, et al. Prolonged sleep deprivation induces a cytokine-storm-like syndrome in mammals. *Cell*. 2023;186(25):5500-5516.e21. doi:10.1016/j.cell.2023.10.025

96. Vaughen JP, Theisen E, Rivas-Serna IM, et al. Glial control of sphingolipid levels sculpts diurnal remodeling in a circadian circuit. *Neuron*. 2022;110(19):3186-3205.e7. doi:10.1016/j.neuron.2022.07.016

97. Kehelpannala C, Rupasinghe TWT, Hennessy T, Bradley D, Ebert B, Roessner U. A comprehensive comparison of four methods for extracting lipids from Arabidopsis tissues. *Plant Methods*. 2020;16(1):155. doi:10.1186/s13007-020-00697-z